# NANO-SCALE CONSIDERATIONS FOR SHALE GAS FLOW SIMULATION

A Thesis

by

ERDEM YALCIN

Submitted to the Office of Graduate and Professional Studies of
Texas A&M University
in partial fulfillment of the requirements for the degree of

MASTER OF SCIENCE

| | |
|---|---|
| Chair of Committee, | John E. Killough |
| Committee Members, | I. Yucel Akkutlu |
| | Maria Barrufet |
| Head of Department, | A. Daniel Hill |

December 2015

Major Subject: Petroleum Engineering

Copyright 2015 Erdem Yalcin

# ABSTRACT

This study basically focuses on numerical simulation of shale gas flow. To be able to capture the complex nature of shale gas reservoirs, different storage and flow mechanisms must be taken into consideration.

Shale reservoir medium consists of organic matter (kerogen), inorganic matter, natural fractures, and hydraulic fractures. In this medium, Darcy flow is not fully capable of modeling shale gas flow since there is different flow mechanisms due to complex porosity system. In addition, Fickian diffusion and flow from matrix to fractures must be considered. For this purpose, the multiple porosity model is used. To be able to keep the resolution of the micromodel on the reservoir scale simulation, the idea of dynamic apparent permeability is followed.

Storage mechanisms of shale gas is also as complex as flow mechanisms. Gas is not only stored as free fluid in pores and fractures, but also as adsorbed phase at the surface of organic matter. However, fluid properties of free gas in nano-scale pores are different than their original values. Also adsorbed phase occupies considerable amount of pore volume which causes reduction in free gas volume. As pore pressure decreases throughout the reservoir life, desorbed gas will be produced with free gas. Thus better understanding of this adsorbed gas behavior within organic matter is the key for accurate modeling of desorption and total gas production.

The proposed workflow is first integrating desorption to the reservoir model by commercial simulator feature. Second, integrating diffusion using the multiple porosity

model and application of dynamic apparent permeability to upscale the model. Third, different fluid properties are introduced to simulator by defining another PVT region. Finally, occupied pore space by adsorbed phase is introduced by modifying Langmuir parameters.

Results are discussed by comparing different cases with cumulative gas production and average reservoir pressure. Significant difference of the models with and without integrating relevant model and properties shows the importance of the nanoscale considerations and their effect on ultimate recovery calculations. Decreasing pore size has a strong effect on gas formation volume factor and viscosity. It causes a decrease on cumulative gas production and average reservoir pressure.

Nano-scale effects have a huge impact on both cumulative gas production and reservoir pressure. As a result, accurate modeling and reducing uncertainity require special attention on desorption, diffusion, pore size effect, and pore volume correction.

ACKNOWLEDGEMENTS

I would like to thank my committee chair, Prof. Killough, and my committee members, Prof. Akkutlu and Prof. Barrufet, for their guidance and support throughout the course of this research.

Thanks also go to my friends and colleagues and the department faculty and staff for making my time at Texas A&M University a great experience. I also want to extend my gratitude to the Turkish Petroleum Corporation, which provided the funding for graduate education.

Finally, thanks to my mother and father for their encouragement and to my wife for her patience and love.

# NOMENCLATURE

| | |
|---|---|
| BHP | Bottom hole pressure, Psi |
| $C_g$ | Gas compressibility, 1/Psi |
| D | Gas diffusion coefficient, $ft^2$/second |
| $d_{mf}$ | Nodal distance between matrix and fracture system in micro model, ft |
| $G_s$ | Amount of adsorbed gas, scf/ton |
| $G_{s,new}$ | Corrected amount of adsorbed gas, scf/ton |
| $G_{total}$ | Amount of total gas, scf/ton |
| $K_{app}$ | Apparent permeability, mD |
| $k_h$ | Horizontal permeability, mD |
| $k_v$ | Vertical permeability, mD |
| M | Molecular weight of adsorbed phase, lb/lb-mole |
| P | Block pressure, Psi |
| $P_f$ | Average pressure in the fracture, Psi |
| $P_L$ | Langmuir pressure which is the pressure at $V_L/2$, Psi |
| $P_{L,new}$ | Corrected Langmuir pressure, Psi |
| $P_m$ | Average pressure in the matrix, Psi |
| RSS | Residual sum of squares |
| $q_a$ | Mass of adsorbed on unit volume of media, lbs/scf |
| $q_{mf}$ | Total flow rate from matrix into fracture system, scf/sec |
| $S_g$ | Gas saturation, % |

| | |
|---|---|
| $S_w$ | Water saturation, % |
| TOC | Total organic carbon content (wt %) |
| $V_L$ | Langmuir volume which represents the maximum sorption capacity, scf/lbm |
| WHP | Well head pressure, Psi |
| $\Sigma A_{mf}$ | Total contact area between the matrix bulk and the fracture system, $ft^2$ |
| $\varphi$ | Porosity, dimensionless |
| $\varphi_s$ | Reduced porosity by adsorbed phase, dimensionless |
| $\rho_g$ | Gas density, lbm/scf |
| $\rho_s$ | Adsorbed phase density, lbm/scf |
| $\overline{\mu_{mf}}$ | Average gas viscosity in the micro scale model, Pa-sec |

TABLE OF CONTENTS

Page

LIST OF FIGURES

Page

LIST OF TABLES

Page

# CHAPTER I

## INTRODUCTION

There has been a sudden decline in oil and gas prices recently. Due to the uncertainty, prices are still remaining low. Inescapable effect of this trend to oil and gas industry is recession by all means. One of the most remarkable results is active rig count. The decrease in the United States can be seen in Figure 1. Shale plays are also affected by this trend as it is expected because of high costs of the horizontal wells and multistage fracturing completion.

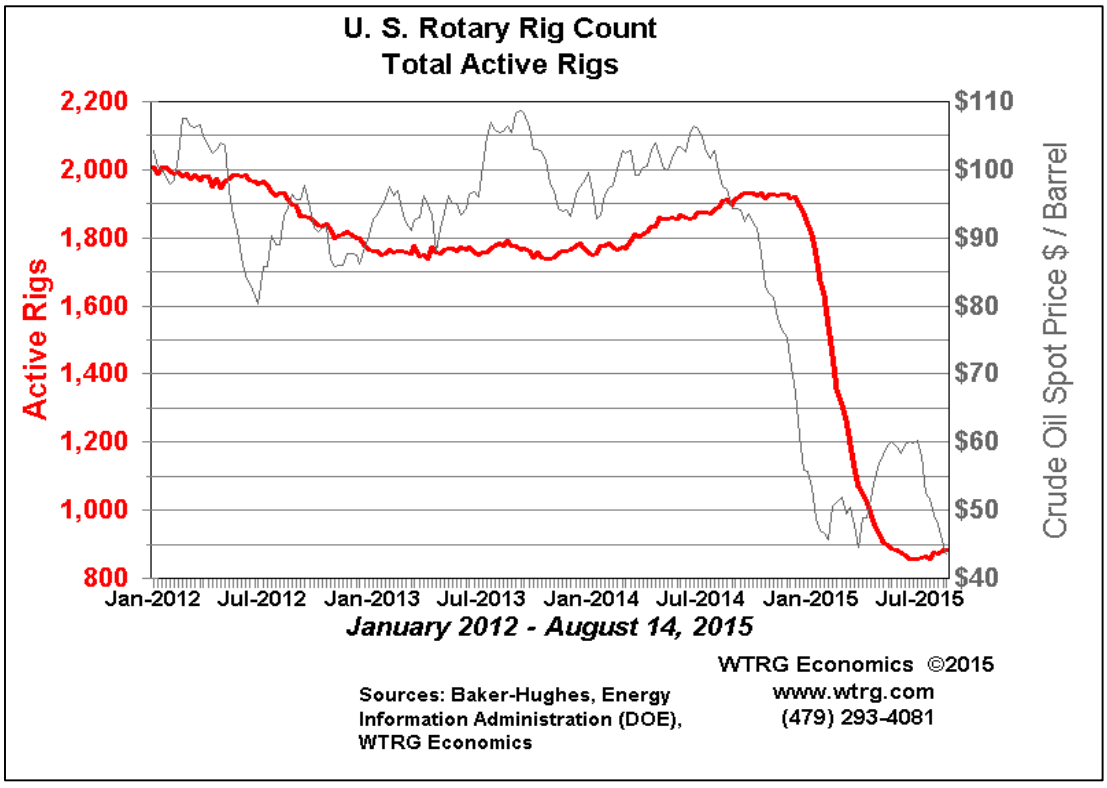


**Figure 1 U.S. Total active rig count (Williams 2015)**

These results force the industry to adapt a new and challenging environment. Accurate modeling of shale gas reservoirs are becoming much more important to reduce the cost of further scenarios. Studies on shale petrophysics and characterization help to better understand shale gas reservoirs for this purpose.

Shale is fine grained, laminated, clastic sedimentary rock. Unlike other sedimentary rocks, shale is both source and reservoir rock. It consists of inorganic matter, organic matter (kerogen) and pore volume (Passey et al. 1990). It is shown by high pressure mercury tests that nano-pores are dominant in shale matrix (Javadpour et al. 2007). Although pore sizes and permeability are very low in both kerogen and inorganic part, there is also natural fracture network in shale reservoirs due to fissility (Carlson et al. 1991). These natural fractures are connected to wellbore through developed hydraulic fractures.

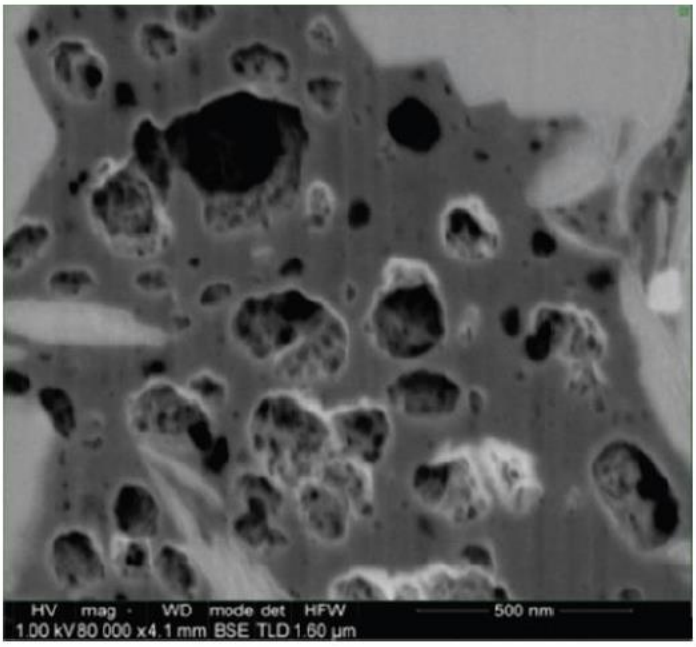


**Figure 2 Organic matter with varying pore sizes (Curtis et al. 2010)**

The storage mechanism of shale gas reservoirs is not only free gas stored in pores and fractures as it is in conventional reservoirs. In addition to free gas, there is also adsorbed gas attached to large internal surfaces of the organic material. The adsorbed amount of gas plays an important role in shale reservoirs as total organic carbon content increases (Hill et al. 2000). Although it is much less compared to adsorbed gas, there is also absorbed (dissolved) gas in organic nano-pores, in hydrocarbon liquid and in water (Boyer et al. 2006).

Due to the extremely low permeability in shale matrix, Darcy Law is limited and not capable to model the flow mechanism in nanometer scale pore sizes. Ertekin et al. (1986) proposed a dual mechanism approach considering both Darcy flow and Fickian diffusion in matrix to characterize coal and shale formations through the dynamic gas slippage factor. Apparent permeability concept is introduced by Javadpour (2009) based on Knudsen diffusion, slippage flow, and advection flow. Later, another model was proposed considering desorption from kerogen surfaces since adsorbed gas is being produced as pressure decreases based on Langmuir isotherm (Shabro et al. 2012).

To be able to capture complex flow mechanism of shale gas reservoir, Yan et al. (2013b) proposed the microscale multiple porosity model since dual porosity/permeability models are not capable of handling flow dynamics in the shale pore network. It is suggested to divide the shale matrix into organic, inorganic, and natural fracture part. Desorption only occurs in organic part depending on total organic carbon content. Further the multiple porosity model is proposed to establish continuum between these parts. According to this idea, nano-pores in organic grids are only

connected to the vugs in organic part. Other porosity systems are connected to the organic part through these vugs as it shown in Figure 3. Since the porosity is too low for Darcy flow in nano-pores in the organic part, the flow mechanism from nano-pores to vugs is modeled based on diffusion. From vugs to fracture network, both Fickian diffusion and Darcy law must be used to model flow dynamics. Flow through fractures are modeled by Darcy flow.

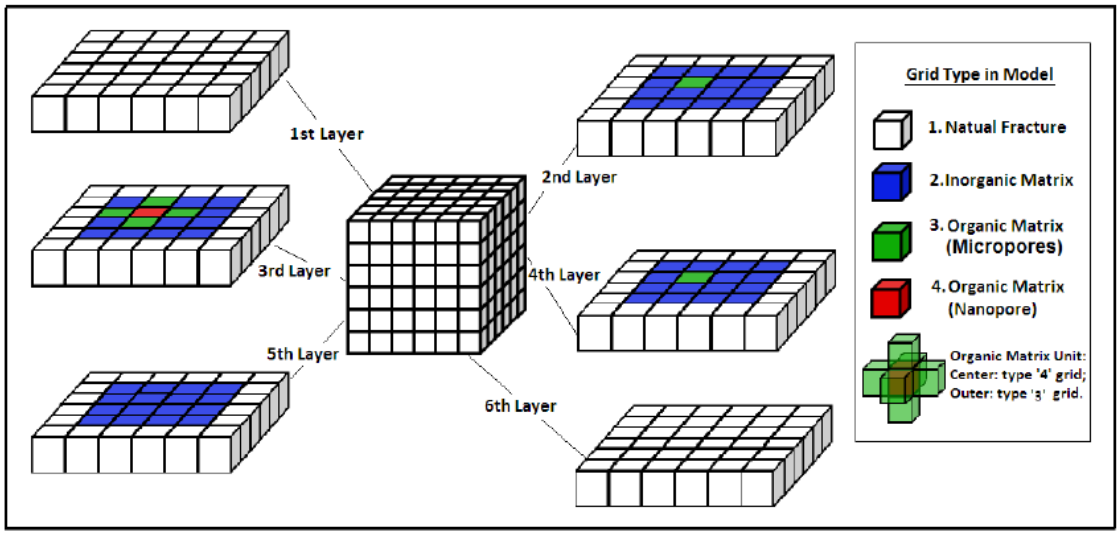


**Figure 3 Micro scale multi porosity model grid system (Yan et al. 2013)**

Although the model is established on micro scale, an upscaling method is proposed to use this model in commercial simulators in reservoir scale (Yan et al. 2013a). The method is based on the idea of apparent permeability which takes into account a coefficient depending on the interaction between matrix and fracture. By this, micro scale model can be upscaled using variable apparent matrix permeability ratio.

Farid (2015) showed that the model can be applied to reservoir scale using dynamic apparent permeability idea by defining apparent permeability ratio through rock compaction tables in any numerical simulator.

It is stated that fluid properties behavior deviate from their expected characteristics depending on pore size in organic rich shales (Didar et al. 2013). In this case, PVT values should be adjusted for matrix part of the reservoir to capture fluid properties correctly depending on experimental values.

Considering storage mechanism of shale, a new petrophysical model proposed by (Ambrose et al. 2012). According to that model, some of the free gas volume is occupied by the adsorbed gas volume. For gas in place calculations, this portion must be taken into consideration as shown in Figure 4.

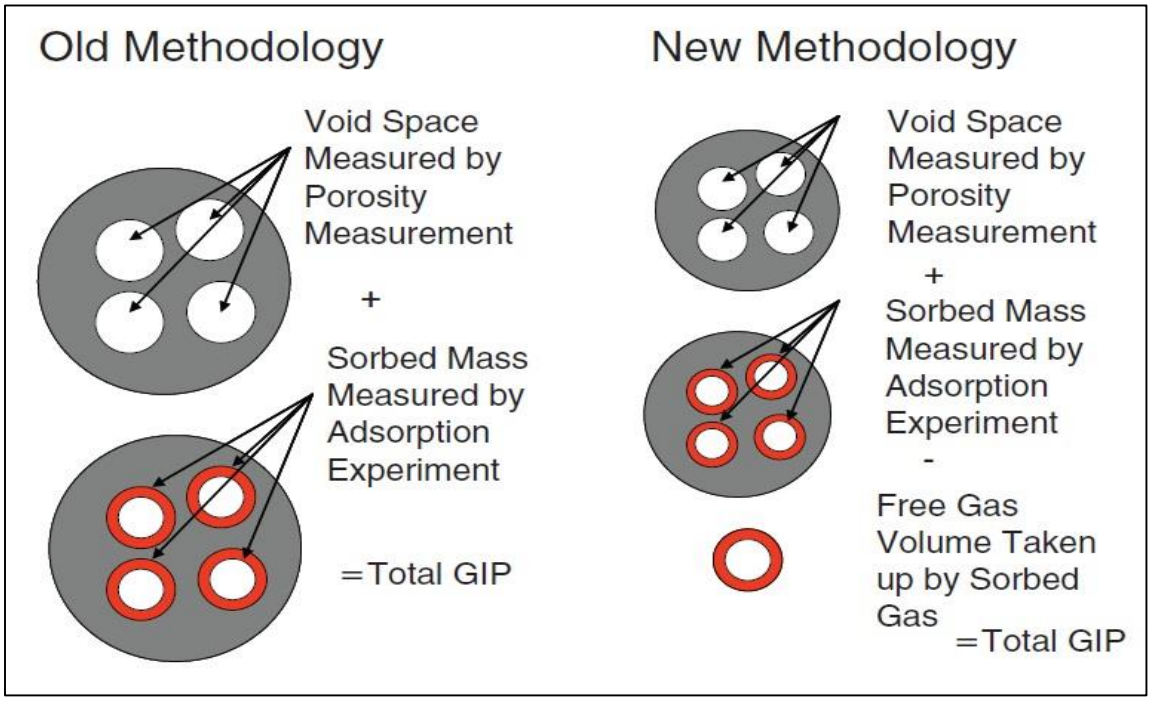


**Figure 4 New methodology for predicting shale gas in place calculations (Ambrose et al. 2012)**

Later, Santos et al. (2013) showed the effect of adsorbed phase to pore volume depending on pressure. Since decreasing pressure causes desorption throughout the life of reservoir, desorbed amount of gas will be produced with free gas and previously occupied pore volume by adsorbed gas will be available as shown in Figure 5. This process will affect the pore volume dynamically as much as pore compressibility (Figure 5). Thus, this effect must be incorporated into simulation studies.

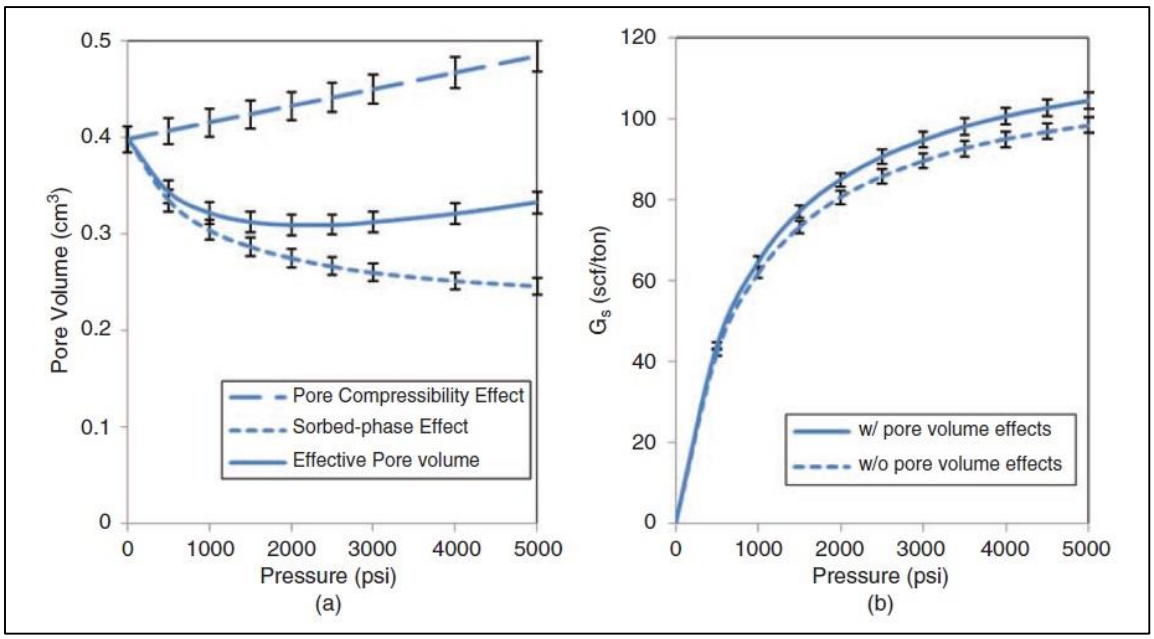


**Figure 5 Effect of desorption on pore volume (Santos et al. 2013)**

In this study, the effect of desorption on pore volume and the pore size effect on fluid properties will be investigated by working in reservoir scale following up the work done in micro scale model. A numerical simulator will be used for this purpose.

Initial reservoir model includes a horizontal well with hydraulic fractures and natural fracture network connected to organic and inorganic part of the reservoir which

is producing in Barnet shale. Desorption process will be modeled by considering Langmuir Isotherm based on total organic carbon content values. Default features of the numerical simulator will be used for this purpose. Fickian diffusion, Darcy flow, and the transient effect between matrix and fracture will be integrated to the reservoir model using the idea of dynamic apparent permeability. To be able to do that, rock compaction tables will be used to enter the apparent permeability ratio values.

Pore size effect will be incorporated into the simulator using another PVT table for matrix part of the reservoir. PVT values are based on the experimental results from a previous study.

Considering desorption effect on pore volume, default features of the numerical simulator is not enough. Also, rock compaction tables are not able to capture the changes on pore volume depending on desorption process since decreasing pore pressure causes an increase in pore volume. To handle this, Langmuir parameters will be adjusted using numerical solver to mimic pore volume change.

Finally, history matching study will be done to show the improvement on the reservoir model. Following, production forecast will be represented to show differences on the production rate and reservoir pressure.

The thesis has been divided into five chapters. Chapter I introduces the basics of modelling gas flow in shale reservoirs by giving brief overview of the theories developed and their incapability. Chapter II gives the details of the reservoir model by physical and mathematical sense. Also integrating desorption and diffusion process are discussed in this chapter. Chapter III describes how to integrate the effect of desorption

on pore volume and the pore size effect on fluid properties to commercial reservoir simulator to be able to work in reservoir scale. Chapter IV discusses the results of previous chapters through cumulative gas production, history matching, and production forecast. Chapter V concludes the study by highlighting the important results.

# CHAPTER II

# MODEL DESCRIPTION

## 2.1. Physical Model

Barnett shale is one of the unconventional plays in USA, located in Fort Worth Basin in North Texas (Figure 6). It is Mississippian aged organic rich and thermally mature shale which is enclosed by dense limestone units. Newark East Field in Barnett shale contains most of the drilled wells, and it is the largest gas field in Texas with formation thickness varying from 300 feet to 500 feet (Montgomery et al. 2005). The field also contains the horizontal well which will be studied in black oil simulator (CMG-IMEX).

The well is stimulated with a large sand fracture treatment. Induced hydraulic fractures are perpendicular to NE-SW and NW-SE directions. Micro seismic data is used to create the fracture map which can be seen on Figure 7 (Mayerhofer et al. 2006). Micro seismically mapped dots are representing 219 million scf. According to that, fracture network has three wings extending to the south west direction. However, there is only one extension of this network to north east side. The total extent of the fracture network is 3000 feet, and the width of the network is around 350 feet. Although lower Barnett is covered well by the network height, upper Barnett has only some traces of the fracture network.

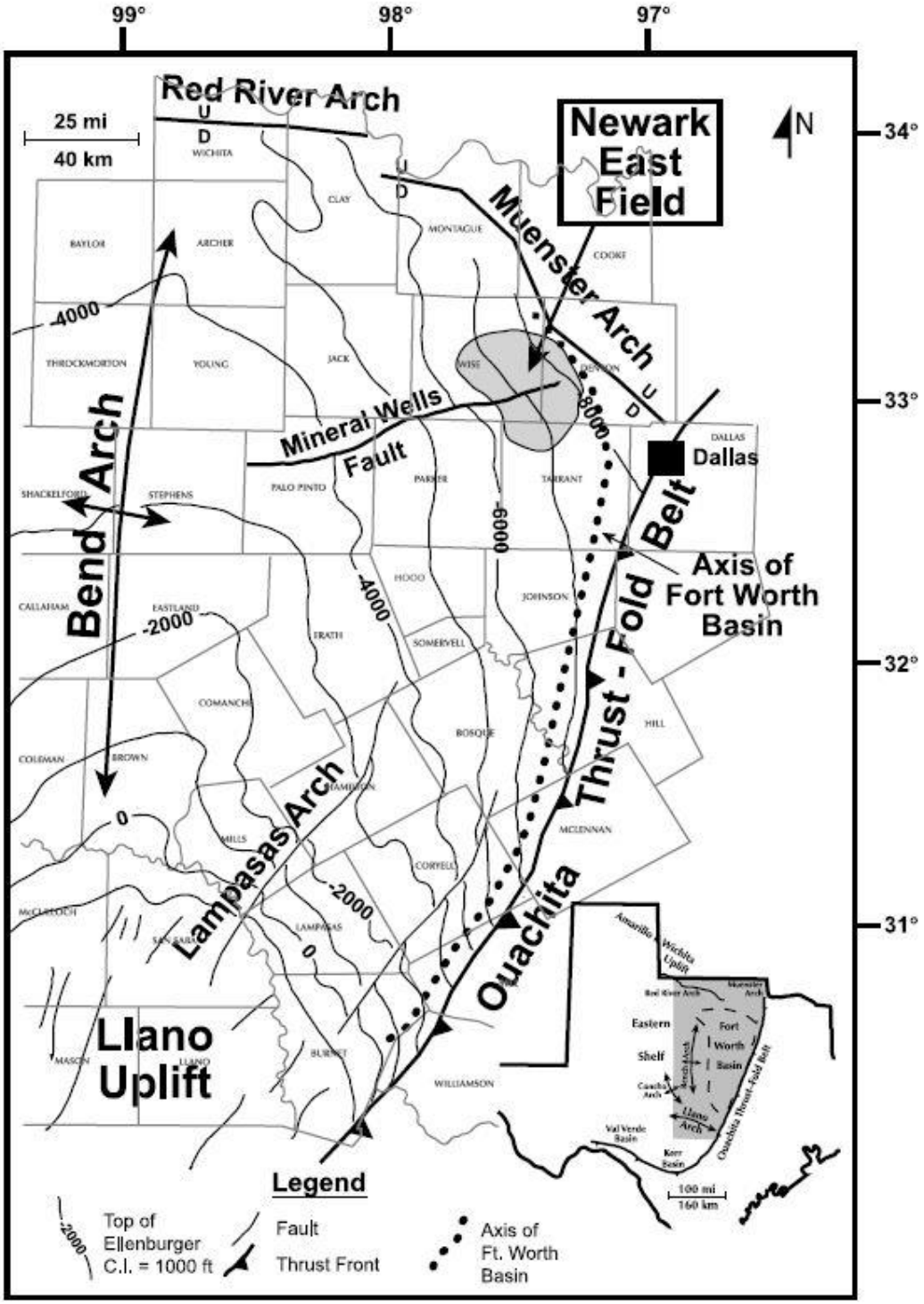


**Figure 6 Fort Worth Basin map (Montgomery et al. 2005)**

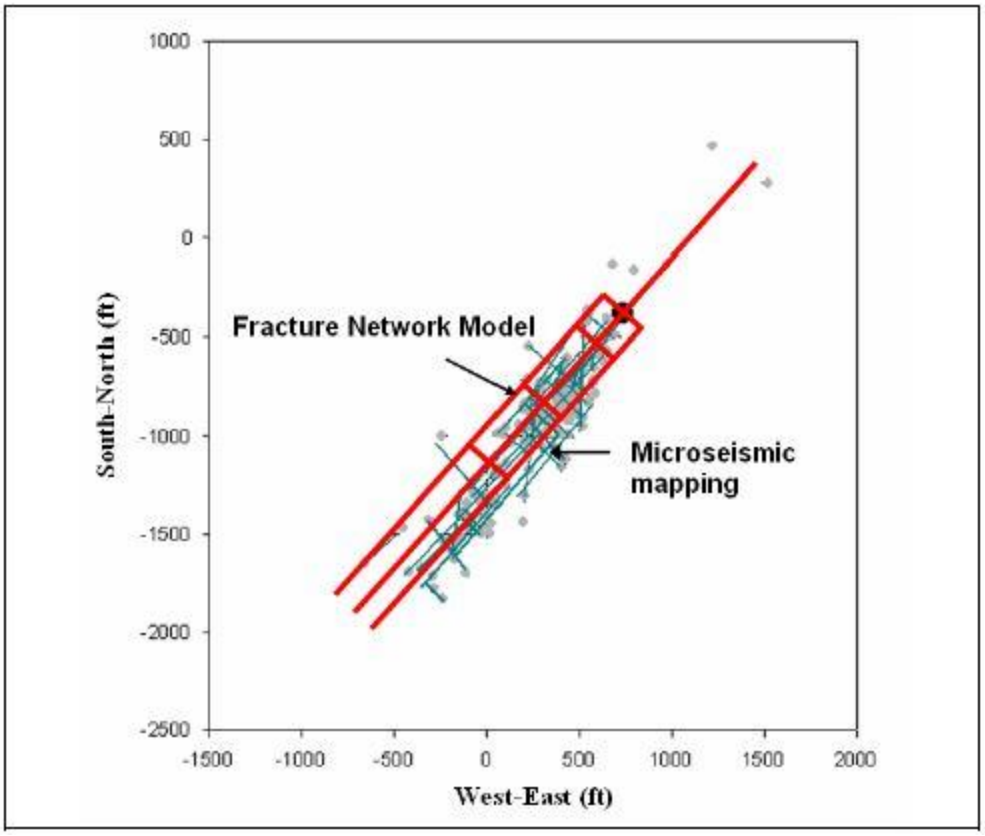


**Figure 7 Fracture network map determined from micro seismic data (Mayerhofer et al. 2006)**

The model consists of dry gas and water with different saturation values for matrix and fracture. The dimension of the SRV is 3200×660×415 scf. 111×145×1 grid represents the SRV. There are two different sets of fractures which represent natural and hydraulic fractures. Fracture width is 0.1 ft for all fractures in the model. For fracture and matrix parts, different rock types, relative permeability curves, and compaction tables are assigned. Reservoir parameters for the initial reservoir model can be seen on Table 1. The well is produced nearly 8 years with gas rate constraint. Desorption, diffusion, and nano-scale considerations are not integrated to the simulation model yet.

**Table 1 Reservoir parameters for the initial reservoir model.**

| Parameter | Matrix | Hydraulic Fractures | Natural Fractures |
|---|---|---|---|
| Permeability (mD) | 0.001 | 100 | 100 (Set 1), 2 (Set 2) |
| $k_h$ / $k_v$ Ratio | 100 | 1 | |
| Porosity (%) | 6 | 100 | |
| Initial Water Saturation (%) | 30 | 60 | |
| Rock Compaction (1/psi) | 3.0E-6 | 3.0E-7 | |
| Relative Permeability Curve | 1 | 2 | |
| Initial Pressure (psi) | 3800 | | |
| Minimum BHP (psi) | 500 | | |
| Temperature ($^{o}$F ) | 180 | | |
| Gas Gravity | 0.6 | | |
| Depth (ft) | 7000 | | |
| Net Thickness (ft) | 415 | | |

The production data includes gas production rates (scf/day), well head pressure (psi), and water rates (bbl/day). Initial simulation model did not show match as seen in Figures 8-11. Before integrating desorption, diffusion, and nano-scale considerations, initial model is tried to be matched against production data as much as possible. Fracture permeability for both natural and hydraulic fractures, matrix porosity, and minimum bottom hole pressure are varied for this purpose through 500 runs. Although the results are closer to actual field data, they need to be improved. Reservoir parameters for the matched model can be seen in Table 2.

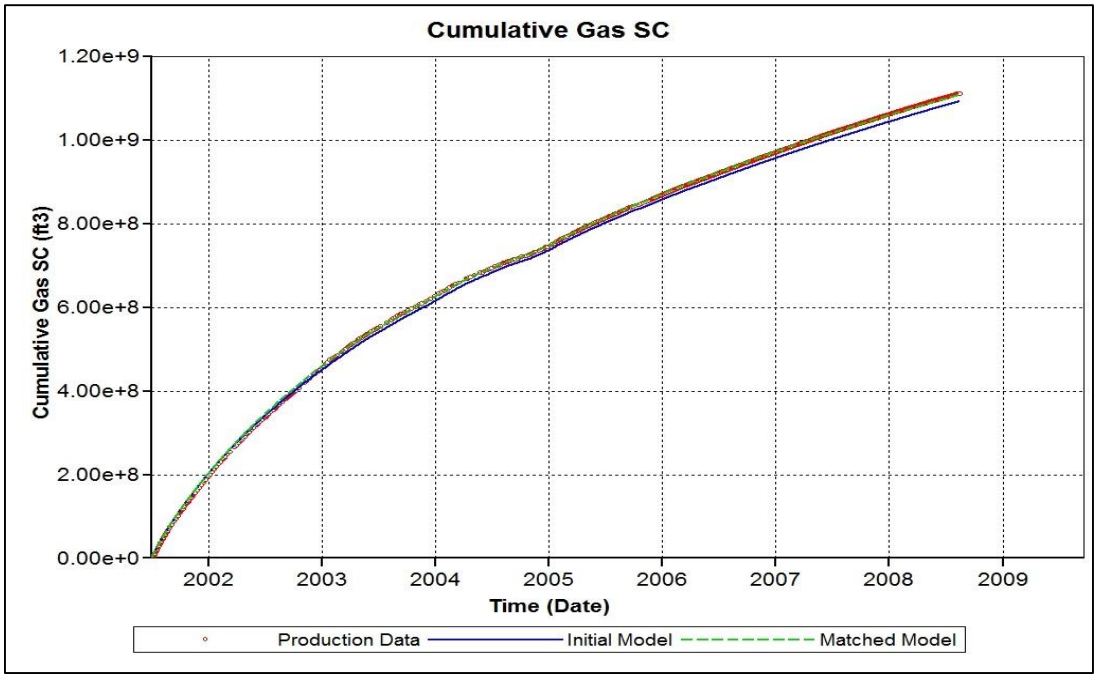


**Figure 8 Cumulative gas production for production data and simulation models**

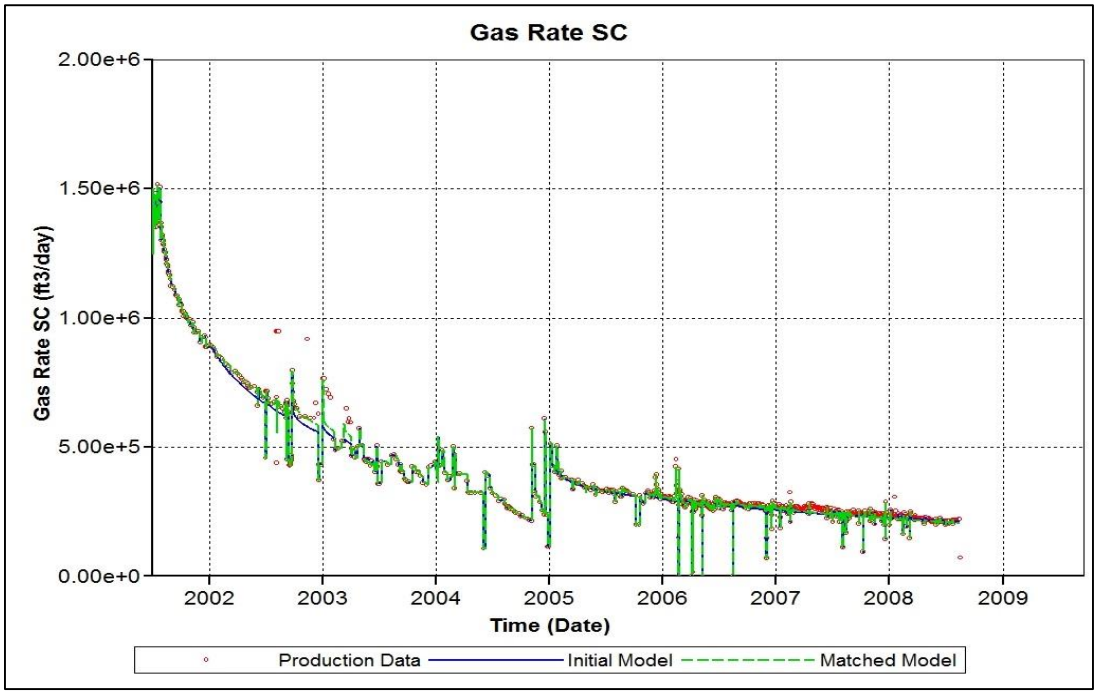


**Figure 9 Gas rate at surface conditions for production data and simulation models**

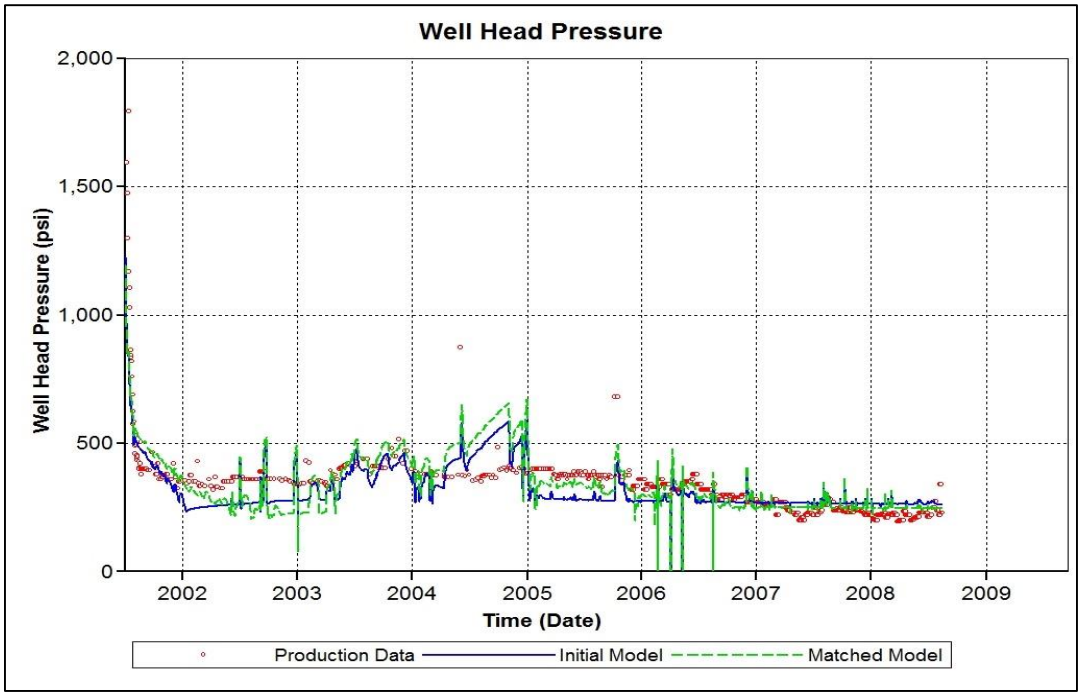


**Figure 10 Well head pressure for production data and simulation models**

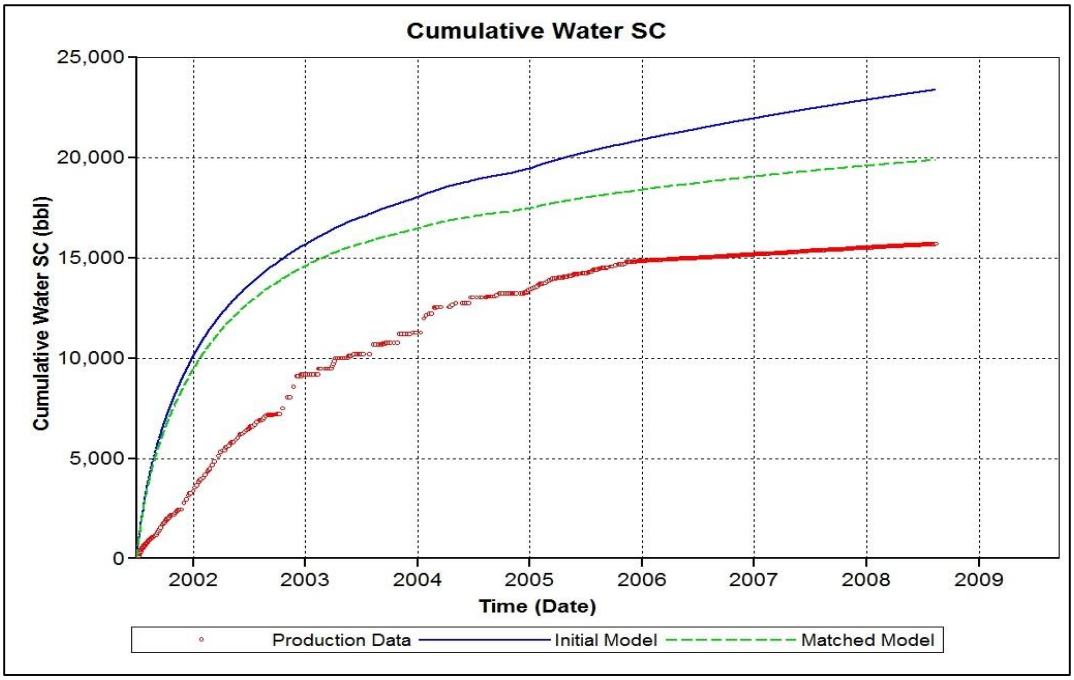


**Figure 11 Cumulative water production for production data and simulation models**

**Table 2 Reservoir parameters for the matched model**

| Parameter | Matrix | Hydraulic Fractures | Natural Fractures |
|---|---|---|---|
| Permeability (mD) | 0.001 | 100 | 100 (Set 1), 2 (Set 2) |
| $k_h$ / $k_v$ Ratio | 100 | 1 | |
| Porosity (%) | 6 | 100 | |
| Initial Water Saturation (%) | 30 | 60 | |
| Rock Compaction (1/psi) | 3.0E-6 | 3.0E-7 | |
| Relative Permeability Curve | 1 | 2 | |
| Initial Pressure (psi) | 3800 | | |
| Minimum BHP (psi) | 393 | | |
| Temperature ($^{o}$F ) | 180 | | |
| Gas Gravity | 0.6 | | |
| Depth (ft) | 7000 | | |
| Net Thickness (ft) | 415 | | |

## 2.2. Mathematical Model

The model consists of four porosity systems. These systems are micro and nano-pores in organic matter with relatively high porosity, inorganic part with low porosity, and fracture network which connects the matrix to wellbore.

In addition to free gas, there is considerable amount of adsorbed gas at the surfaces of organic matter. As pressure decreases, desorbed gas will be produced. Langmuir isotherm is used to model this process. Langmuir equation which includes Langmuir volume and Langmuir pressure as fitting parameters as follows:

$$G_s = \frac{V_L P}{P + P_L} \quad (1)$$

Gas in place calculations for organic rich shales are performed by the following equation in terms of scf/ton (Ambrose et al. 2012):

$$G_{total}=32.0368\frac{\varphi\,(1-S_w)}{\rho_b B_g}+\frac{V_L\,P}{P+P_L} \tag{2}$$

However, adsorbed gas occupies some of the pore volume, and this must be taken into consideration. Ambrose et al. (2012) proposed adsorbed phase correction by following equations:

$$G_{total}=32.0368\frac{\varphi\,(1-S_w)-\boldsymbol{\varphi_s}}{\rho_b B_g}+\frac{V_L\,P}{P+P_L} \tag{3}$$

$$\varphi_s=1.318\times10^{-6}M\frac{\rho_b}{\rho_s}(G_s) \tag{4}$$

Adsorbed phase correction is not only important for gas in place calculations, but also it is important for flow calculations since adsorbed gas amount will be desorbed as pressure decreases. So, occupied pore volume will decrease and available pore volume will increase as pressure decreases. In this case, it is necessary to mimic this process using a pressure dependent reservoir parameter. Following equation is proposed for this purpose:

$$32.0368\frac{\varphi\,(1-S_w)-\varphi_s}{\rho_b B_g}+\frac{V_L\,P}{P+P_L}=32.0368\frac{\varphi\,(1-S_w)}{\rho_b B_g}+\frac{V_{L,new}\,P}{P+P_{L,new}} \tag{5}$$

Equation (5) proposes to calculate a new gas formation volume factor which can capture the effect of desorbed gas on pore volume. This can be done using the residual sum of squares method on Equation (6) by minimizing the error with numerical solvers.

$$RSS=\sum_{i=1}^{n}(G_{s,i}-G_{s,new,i})^2 \tag{6}$$

Considering flow mechanisms, Darcy flow is not capable to model gas flow in nano-pores based on Knudsen number. Thus, free gas and desorbed gas flow in the

nano-pores of organic matter can be modeled by Fick's Diffusion Law. The flow between micro-pores and fractures is modeled by both Darcy flow and Fick's Diffusion Law. Other flow mechanisms are governed only by Darcy flow.

Gas phase mass balance and aqueous phase mass balance can be used for gas and water component respectively. It is assumed that water molecules only exist in aqueous phase, hydrocarbon molecules only exist in the gaseous phase and the solubility of hydrocarbons in the aqueous phase is negligible. It is also assumed that the conditions are isothermal. So, the gaseous phase and aqueous phase equations are as follows:

$$\nabla.\left\{\rho_g\left[DC_g\nabla P+\frac{k\,k_{rg}}{\mu_g}\left(\nabla P_g+\rho_g g\nabla z\right)\right]\right\}=-\frac{\partial\left(\rho_g S_g\varphi\right)}{\partial t}-\frac{\partial[qa(1-\varphi)]}{\partial t} \tag{7}$$

$$\nabla.\left\{\rho_w\left[\frac{k\,k_{rw}}{\mu_w}\left(\nabla P_w+\rho_w g\nabla z\right)\right]\right\}=-\frac{\partial\left(\rho_w S_w\varphi\right)}{\partial t} \tag{8}$$

Where $S_w + S_g = 1$

Fick's second law of diffusion will not be used explicitly in the model. Instead, the idea of dynamic apparent permeability which is proposed by Yan et al. (2013a) will be used. Dynamic apparent permeability is computed as a function of matrix pressure. Diffusion, Darcy flow, and the transition flow between matrix and fractures are incorporated to dynamic apparent permeability as follows:

$$K_{app}=\frac{q_f\,d_{mf}\,\mu_{mf}}{(P_m-P_f)\sum A_{mf}} \tag{9}$$

## 2.3. Integrating Desorption

Adsorption is an important storage mechanism for organic rich shale gas reservoirs. Other than free gas storage depending on available pore volume in conventional reservoirs, gas is adsorbed on the large internal surfaces of organic matter and clay in shale reservoirs. So, adsorption capacity is dictated by the available surface area instead of pore volume (Sing et al. 1985). Organic matter in shale has great adsorption capacity since it has large internal surfaces and affinity to methane.

Langmuir isotherm is the most commonly used approach to model adsorption. After determining Langmuir volume and Langmuir pressure as seen in Figure 12, desorption process can be easily integrated to the simulation model. According to Langmuir model, adsorbed gas is in equilibrium with free gas at high pressures. As pressure decreases, adsorbed gas will be free and produced.

As Langmuir pressure, 2020 psi will be used as it is proposed by Zhang et al. (2012) for Barnett shale. To be able to determine Langmuir volume, first total organic carbon content must be determined since it affects the adsorption capacity.

Passey et al. (1990) proposed a method to determine TOC content depending on well logs. However, there is not available log data for this particular well. Thus, for different TOC values for Barnett Shale in literature, Langmuir volume will be calculated with the following equation which is based on empirical analysis that give a correlation between TOC and Langmuir volume (Zhang et al. 2012):

$$V_L = 1.34\ TOC + 0.0134 \tag{9}$$

Where $V_L$ is in mmol($CH_4$)/g of rock and TOC is in weight percent.

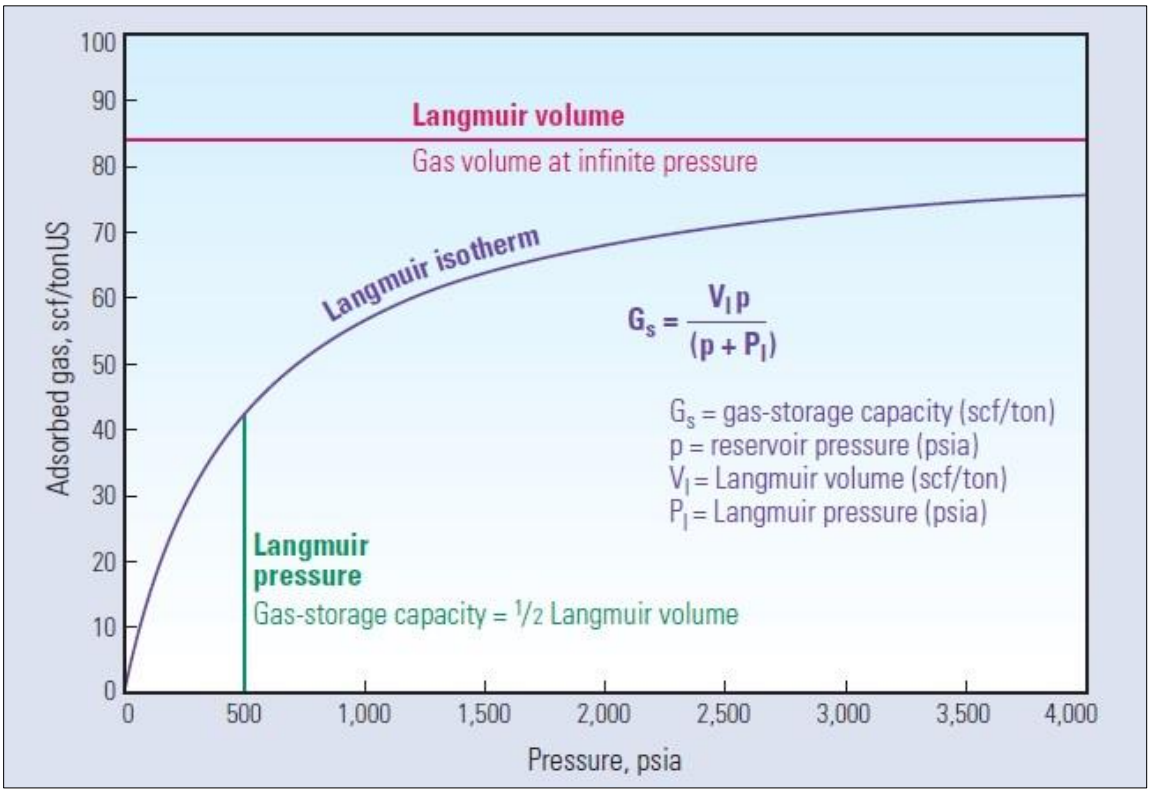


**Figure 12 Langmuir isotherm and input parameters (Boyer et al. 2006).**

The total organic carbon content for Barnett shale is reported by weight percentage from several studies. Average values are 3.16-3.26 by Jarvie et al. (2004), 3.3-4.5 by Montgomery et al. (2005), and 2.4-5.1 by Jarvie et al. (2007). In this study, TOC will be taken as 4%. To analyze the effect of TOC, 7% and 10% values will also be used.

CMG IMEX is able to capture the desorption process. Langmuir volume, Langmuir pressure, and intrinsic rock density are the only input parameters. These input parameters can be seen in Table 3.

**Table 3 Input parameters for desorption in Barnett shale**

| | | | |
|---|---|---|---|
| TOC (%) | 4 | 7 | 10 |
| $P_L$ (psi) | 2020 | 2020 | 2020 |
| $V_L$ (scf/ton) | 47.65 | 75 | 104.83 |
| Rock Density (lbm/scf) | 167.5 | 167.5 | 167.5 |

## 2.4. Integrating Diffusion

To be able to integrate diffusion to the simulation model, the dynamic apparent permeability idea will be used as it is discussed in Chapter I by using equation (8) (Yan et al. 2013). Due to the fact that viscous flow is not the only flow mechanism in nano-meter size pores, apparent permeability deviates from Darcy flow as seen in Figure 13 (Yan et al. 2013). The overlap at high pressure during early time is the sign of dominance of Darcy flow from large pores to fracture system. As pressure decrease reaches to the matrix, the diffusion starts, which causes deviation of apparent permeability from Darcy permeability as it is also discussed by Javadpour (2009). It is important to note that apparent permeability is not dependent on the matrix and fracture size and is hardly affected by desorption.

Fortunately, the proposed dynamic apparent permeability concept can be easily integrated to the simulation model by using rock compaction tables using the apparent permeability ratio in Figure 14 (Yan et al. 2013a). It must be noted that represented apparent permeability is not related to stress dependence of the rock matrix here.

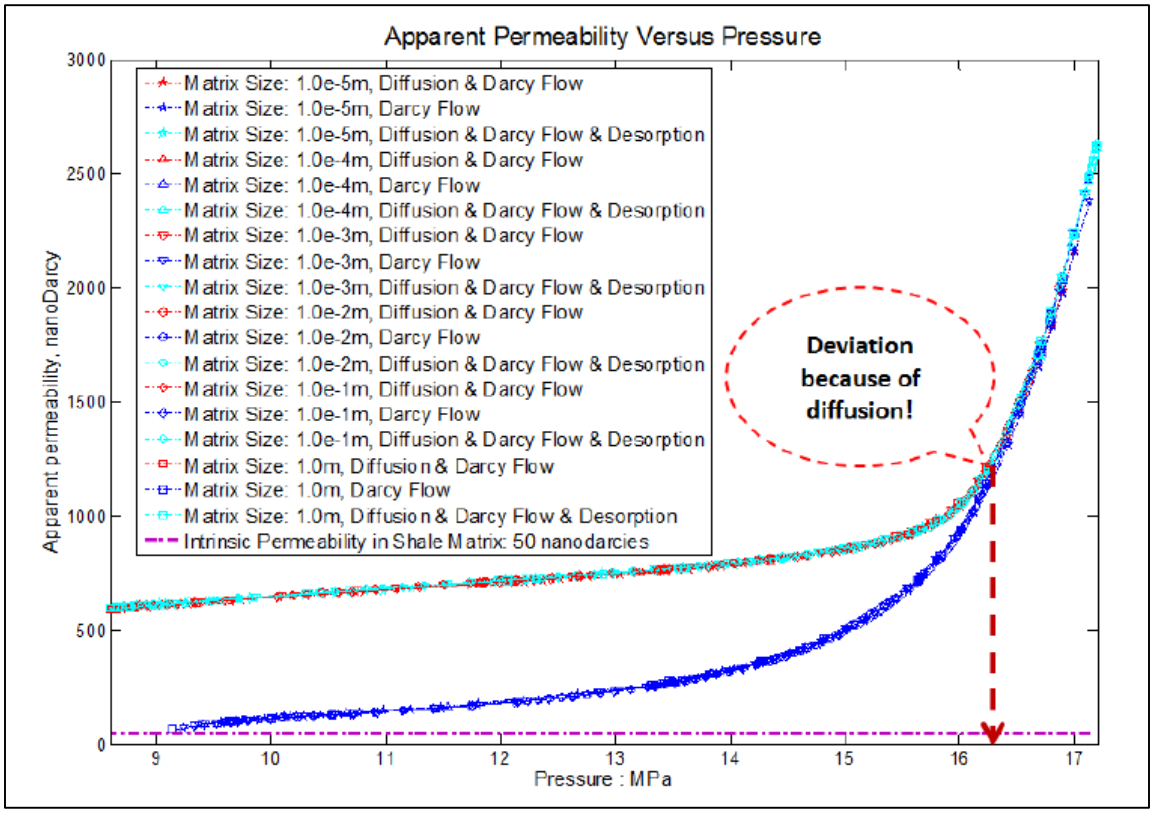


**Figure 13 Apparent permeability versus pressure (Yan et al 2013)**

By integrating diffusion into the simulation model, the micro-scale model will be upscaled using the idea of dynamic apparent permeability. This will help us to investigate the micro-scale considerations on reservoir scale.

Effects and results of integrating desorption and diffusion into the simulation model will be discussed in Chapter IV in detail. Before that, other nano-scale considerations will be discussed and integrated to the model in Chapter III.

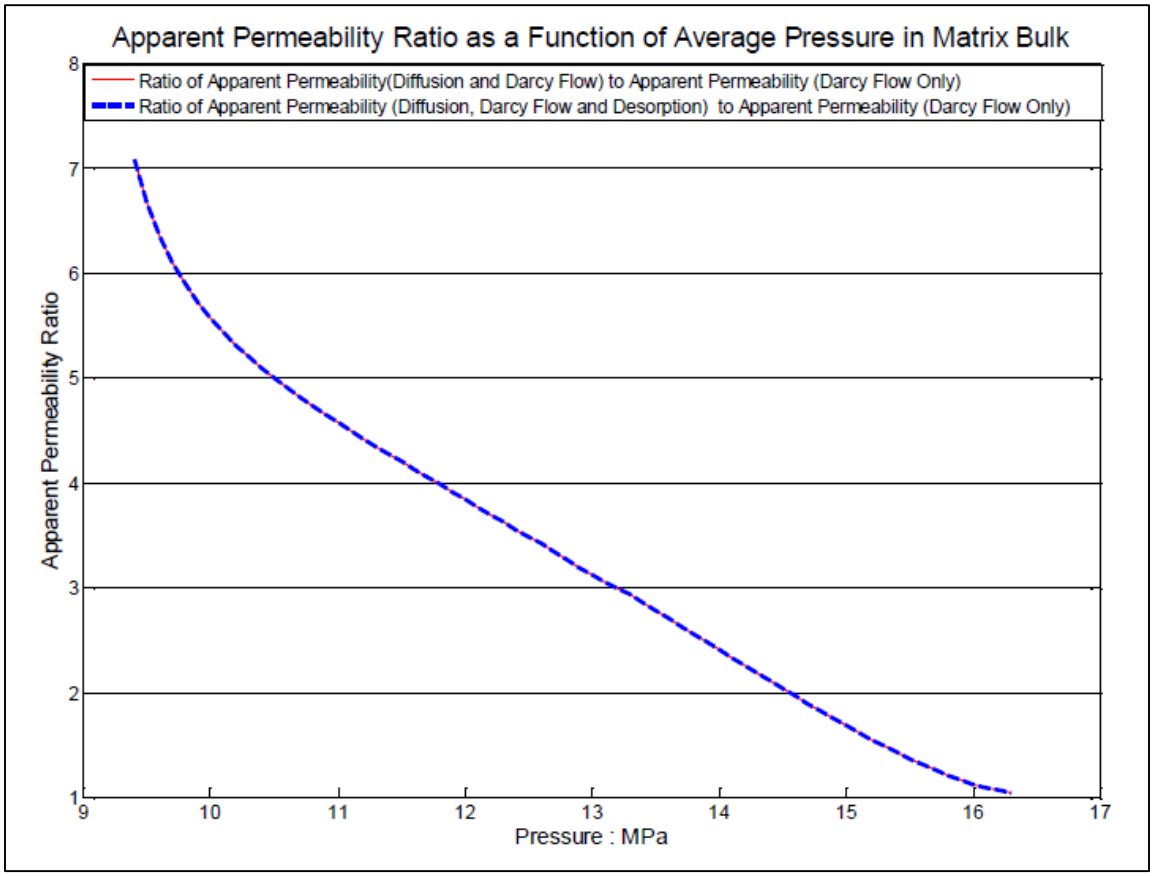


**Figure 14 Apparent permeability ratio as a function of pressure (Yan et al. 2013a)**

# CHAPTER III

# NANO-SCALE CONSIDERATIONS

Desorption and diffusion are relatively well studied topics considering shale gas storage and flow mechanisms. However, there are still ongoing studies investigating pore size scale effects. For accurate understanding and modeling of shale gas flow, it is important to discuss these studies. Moreover, it is necessary to be able to integrate this results to simulation studies in reservoir scale.

## 3.1. Pore Size Dependence of Fluid Properties

Recently, it has been shown by experimental studies that fluid properties are deviating from their expected behavior depending on pore size (Figure 15-17) (Didar and Akkutlu 2013). The reason of this behavior is the decrease of critical temperature and critical pressure of free methane as pore size decreases. This leads to an increase in z-factor and gas formation volume factor which cause an over-estimation of free gas in place of shale reservoirs. Moreover, this phenomenon is affecting flow simulation since these fluid properties are also important parameters to model gas flow.

To be able to introduce deviated fluid properties, another PVT region will be defined for matrix part. Thus, there will be two different sets of fluid properties value for the matrix and fracture part. Original values will be used for the fracture part while deviated values will be used for the matrix part.

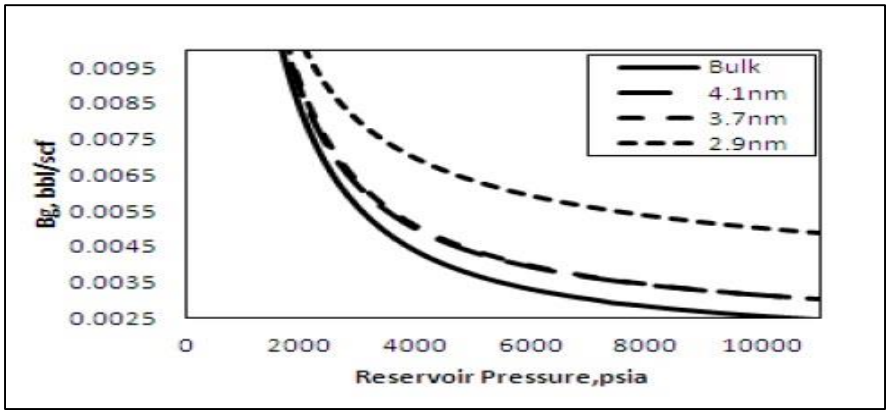


**Figure 15 Pore size dependent methane gas formation volume factor at 180 °F (Didar et al. 2013)**

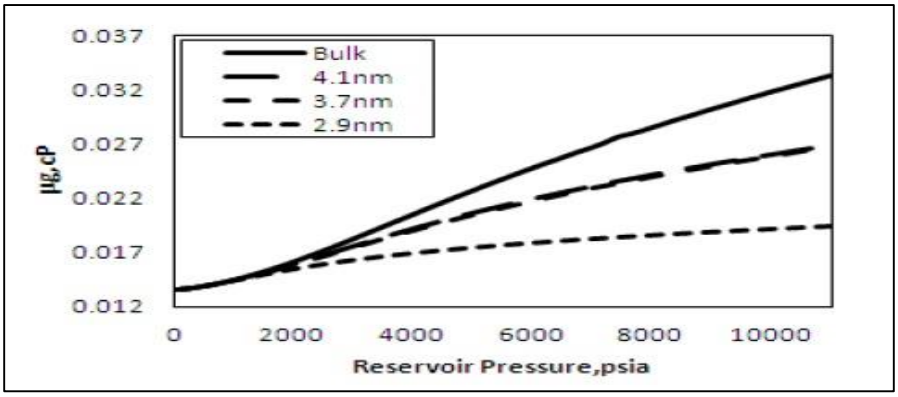


**Figure 16 Pore size dependent methane viscosity at 180 °F (Didar et al. 2013)**

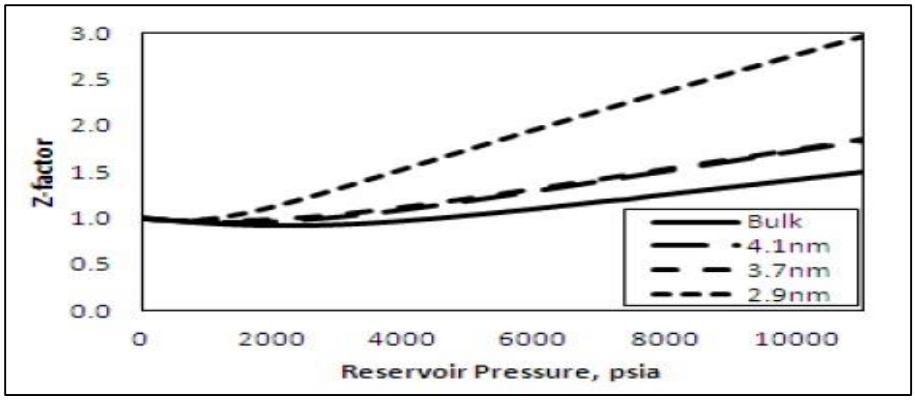


**Figure 17 Pore size dependent z-factor at 180 °F (Didar et al. 2013)**

Since temperature of the experiment is same as the temperature of the reservoir, these results can be integrated to the reservoir model. Another consideration is determining pore width of the reservoir matrix part. Adesida et al. (2011) studied kerogen pore size distribution of Barnett shale using DFT analysis. According to their results which were taken from 3 sample, effective pore widths were determined as 6.78 nm, 4.86 nm, and 5.50 nm. However, 4.1 nm was assumed as effective pore width for the simulation model since it was the closest value which was studied by Didar et al. (2013). The 2.9 nm pore width was also studied to show the pore size effect.

The gas formation volume factor values were extracted from Figure 15 using plot digitizing tools. However, instead of the gas formation values, gas expansion factor was entered to simulator input file for practical purposes. The difference between bulk expansion factor and pore size affected expansion factor in the kerogen part can be seen in Figure 18.

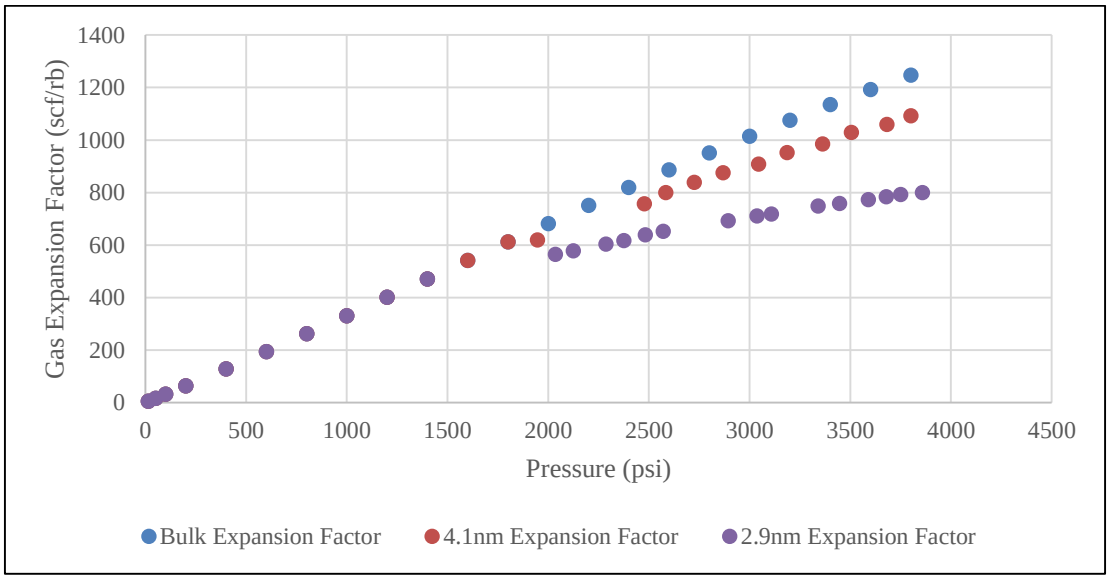


**Figure 18 Gas expansion factors with and without pore size effect**

It is important to note the deviation starting after 1800 psi. As it can also be seen in Figure 15, the pore size effect is greater at higher pressures.

The gas viscosity values are extracted from Figure 16 by using the same tool. The deviation from bulk values can be seen after 1800 psi as well in Figure 19.

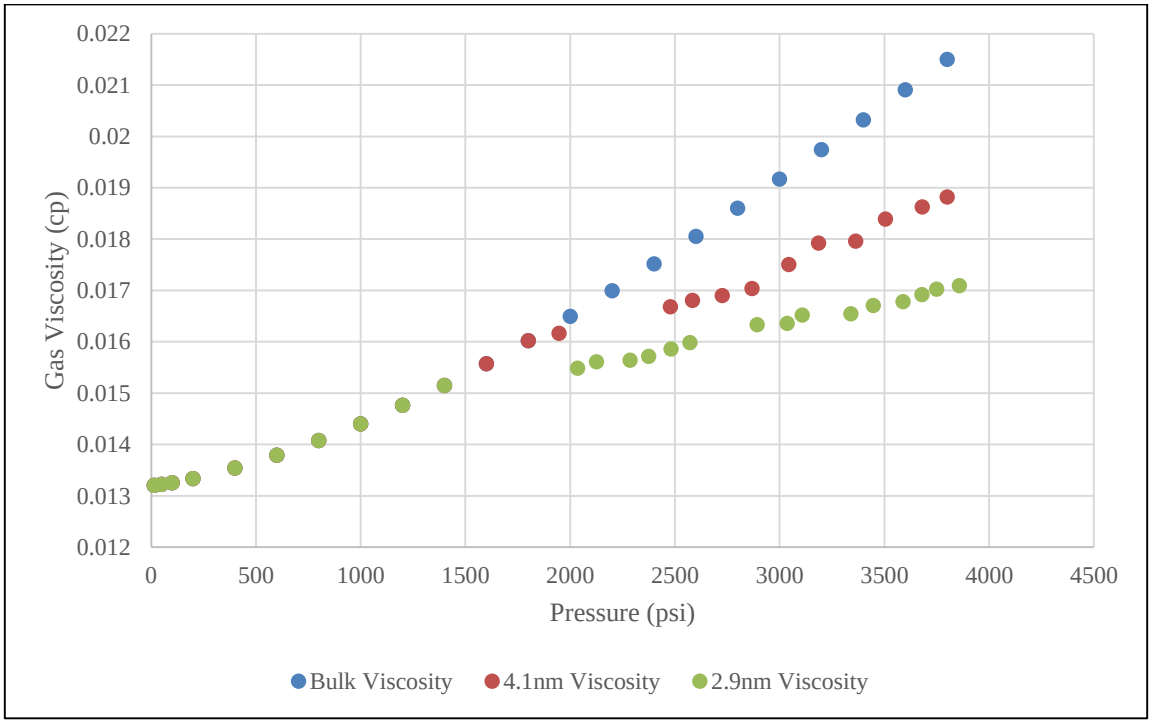


**Figure 19 Gas viscosity with and without pore size effect**

CMG IMEX also uses gas expansion factor to calculate Z-factor. Since it is derived from the PVT table in the input file, it is not entered explicitly. Gas density is entered only for stock tank conditions, and it is calculated using PVT table as well. So, gas expansion factor and gas viscosity are the only needed parameters to input explicitly.

### 3.2. Adsorption Effect on Pore Volume

As it is noted in Chapter I, adsorbed gas on the internal surfaces of kerogen occupies some of the pore volume and it causes a decrease on available pore volume at initial conditions. Ambrose et al proposed a new petropyhsical model to consider this phenomenon for gas in place calculations (Figure 20).

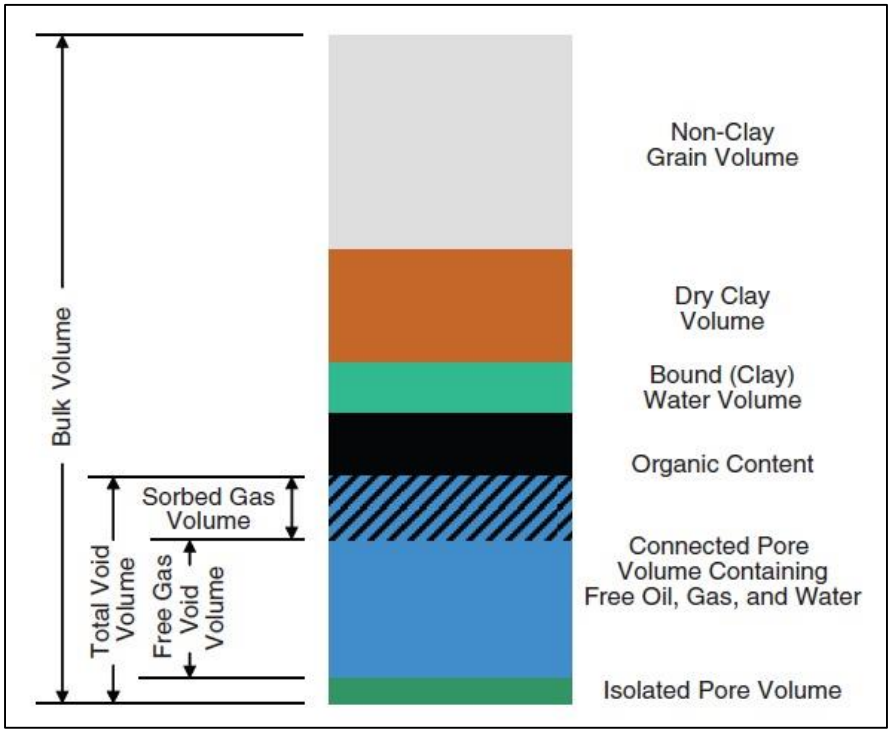


**Figure 20 New petrophysical model for shale gas reservoirs proposed by Ambrose et al. (2012)**

However, the occupied volume is not constant throughout the life of reservoir since adsorbed gas will be produced with free gas as pressure decreases, and it leads to an increase in free gas void volume. Santos et al. (2013) studied the pore volume effect of adsorbed phase depending on pressure. Thus, accurate flow simulation of shale gas reservoirs requires integration of this phenomenon.

To be able to integrate the pore volume effect of adsorbed phase, a new technique is proposed based on modifying Langmuir parameters by Equation (5). According to this equation, pore volume correction on the left hand side of the equation will serve to calculate new Langmuir parameters on the right hand side. First, corrected free void volume calculated with left hand side. Second, the void volume is calculated using right hand side. After that, the results from left hand side equalized to results from right hand side by changing Langmuir parameters. Residiual sum of squares method which is given by Equation (6) is used for this.

By doing this, the changing pore volume will be taken into consideration. In other words, modified Langmuir parameters mimics the effect of desorption on pore volume.

Langmuir isotherms can be seen in Figure 21-23 for different TOC values. As it is expected, adsorbed gas volume is increasing as TOC increases. Original Langmuir isotherm is shown without the effect of pore volume correction. After integrating pore volume correction, adsorbed gas volumedecreases significantly on modified Langmuir isotherm. Adjusting Langmuir parameters for the best match with modified Langmuir isotherm gives input Langmuir isotherm. This is the isotherm which is integrated to the simulation through Langmuir parameters.

In Chapter IV, results will be discussed in reservoir scale. Simulation model will be updated step by step considering pore size effect and the effect of adsoption on pore volume.

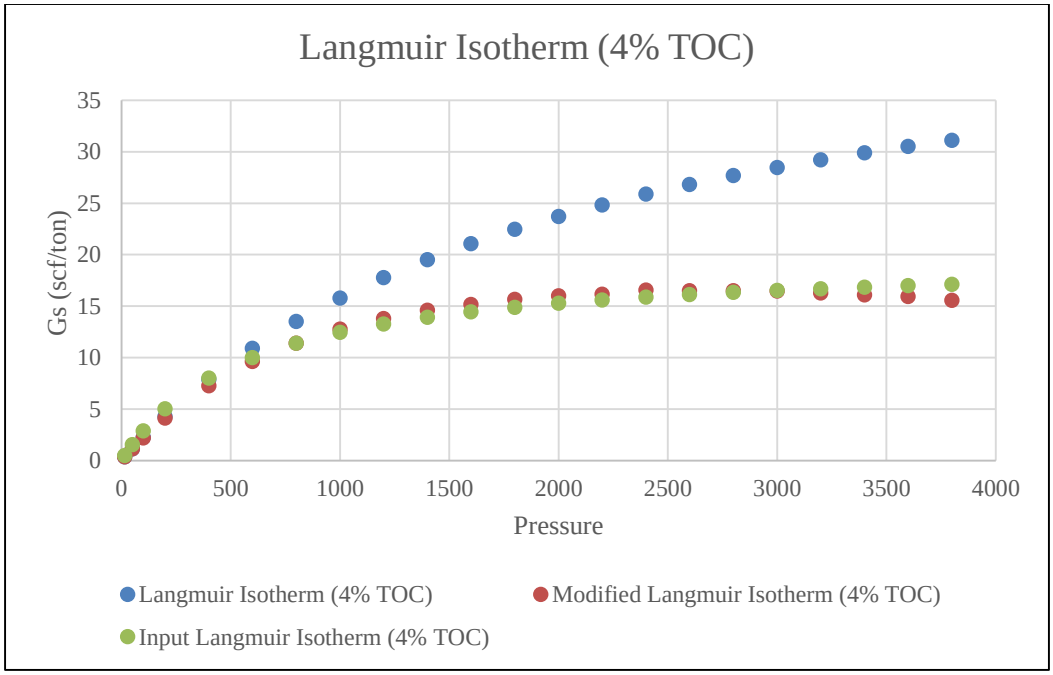


**Figure 21 Langmuir isotherm with and without pore volume correction for 4% TOC**

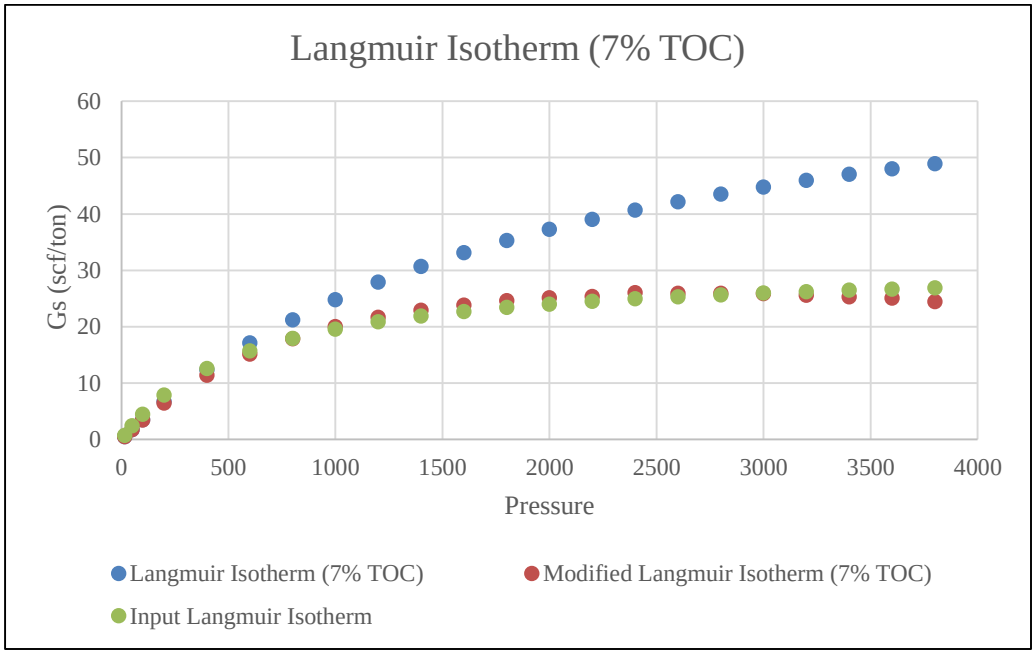


**Figure 22 Langmuir isotherm with and without pore volume correction for 7% TOC**

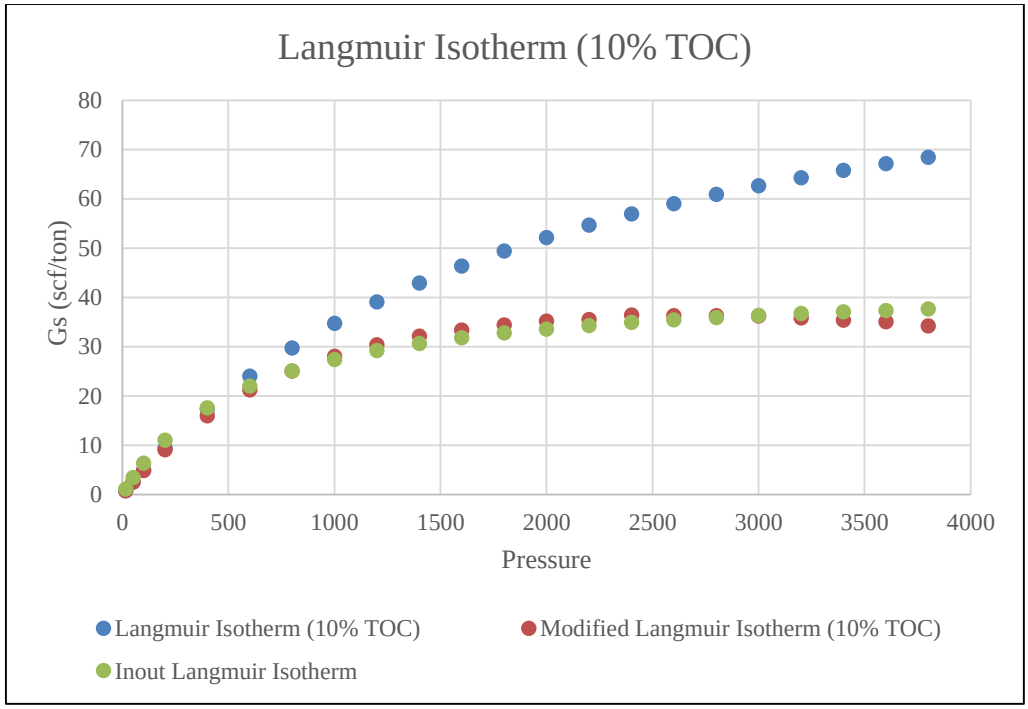


**Figure 23 Langmuir isotherm with and without pore volume correction for 10% TOC**

# CHAPTER IV

# RESULTS AND ANALYSES

In this chapter, different cases are compared in reservoir scale. Desorption, diffusion, pore size dependent fluid properties, and pore volume correction are discussed in terms of cumulative gas production and average reservoir pressure.

## 4.1. Desorption

As it is discussed in Chapter III, desorption is integrated to the simulation model by Langmuir parameters. 3 different cases are run to see the effect of TOC. At this point, diffusion, pore size effect, and pore volume correction are not integrated to the model yet. Since the well is producing on surface gas rate constraint, it is not possible to observe the effect of desorption on cumulative gas production. To be able to capture the effect of desorption for different TOC values, primary constraint is changed to bottom hole pressure.

Effect of different TOC values on cumulative gas production against base case can be seen in Figure 24. It is important to note the overlap at early times of the reservoir. Adsorbed gas cannot be produced at early times since high reservoir pressure does not allow desorption. However, as pressure decreases, deviation starts and effect of desorption can be seen clearly. As TOC increases, cumulative gas production also increases since there is more desorbed gas.

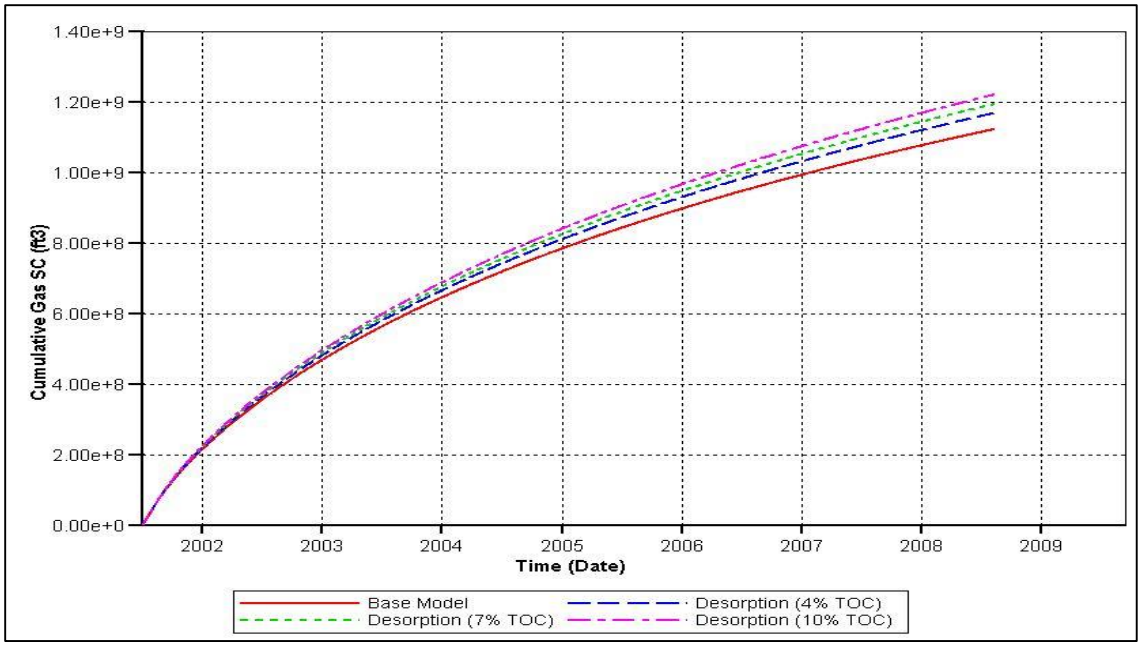


**Figure 24 Cumulative gas production for different TOC against the base case.**

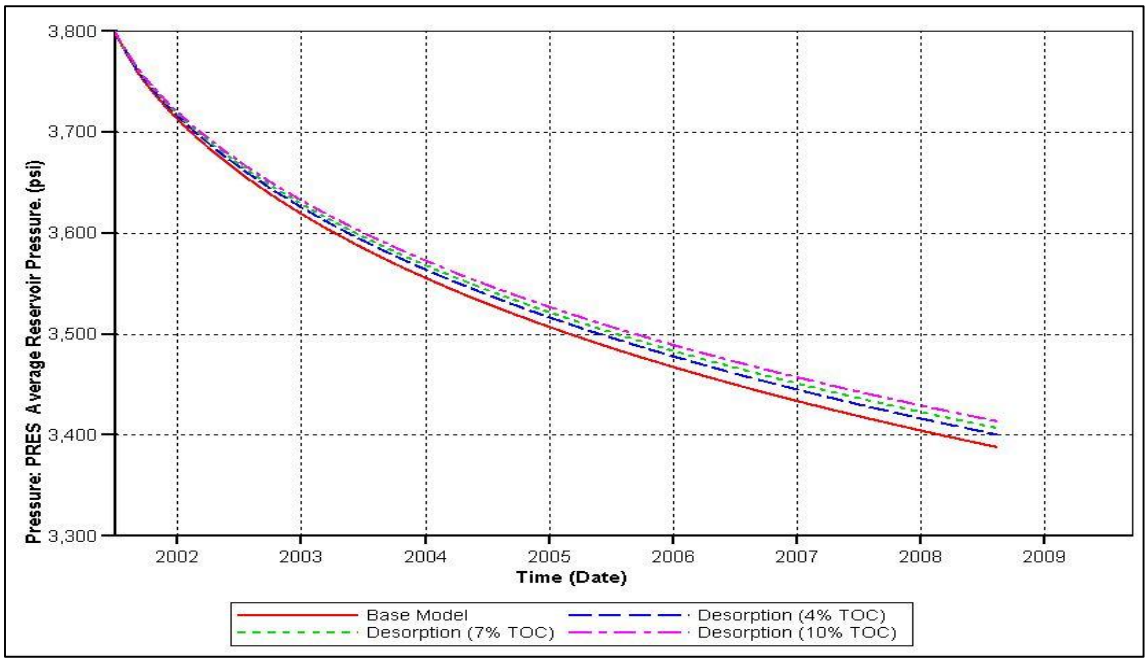


**Figure 25 Average reservoir pressure for different TOC against the base case.**

Average reservoir pressure profiles for different TOC values against base case are shown in Figure 25. Likewise cumulative gas production, there is also an overlap on average reservoir pressure. After deviation starts, higher TOC values maintain higher reservoir pressures as the amount of desorbed gas increases.

## 4.2. Diffusion

As it is discussed in Chapter III, diffusion is the only mechanism which causes flow from nano-pores. Additionally, flow from micro-pores is modelled by both diffusion and Darcy flow. Therefore, it is necessary to integrate diffusion into the simulation model in order to model gas flow from nano-pores system. After the rock compaction tables are modified to capture dynamic apparent permeability, several runs are made to compare different cases. To be able to see the effect of diffusion, first desorption is turned off and the model is run with diffusion only. After that, both desorption and diffusion case are run. Base model and desorption only model are also shown to compare the cases.

Cumulative gas production for these cases can be seen in Figure 26 with BHP as primary constraint. First thing to note here is the great increase on ultimate recovery when diffusion is turned on. This result is consistent with the theoretical approach since diffusion is the only mechanism draining gas from nano-pore system. Deviation from base model and desorption only model starts at early times as the well starts to produce. Desorption still helps to increase the cumulative gas production. However, its effect is limited with respect to diffusion.

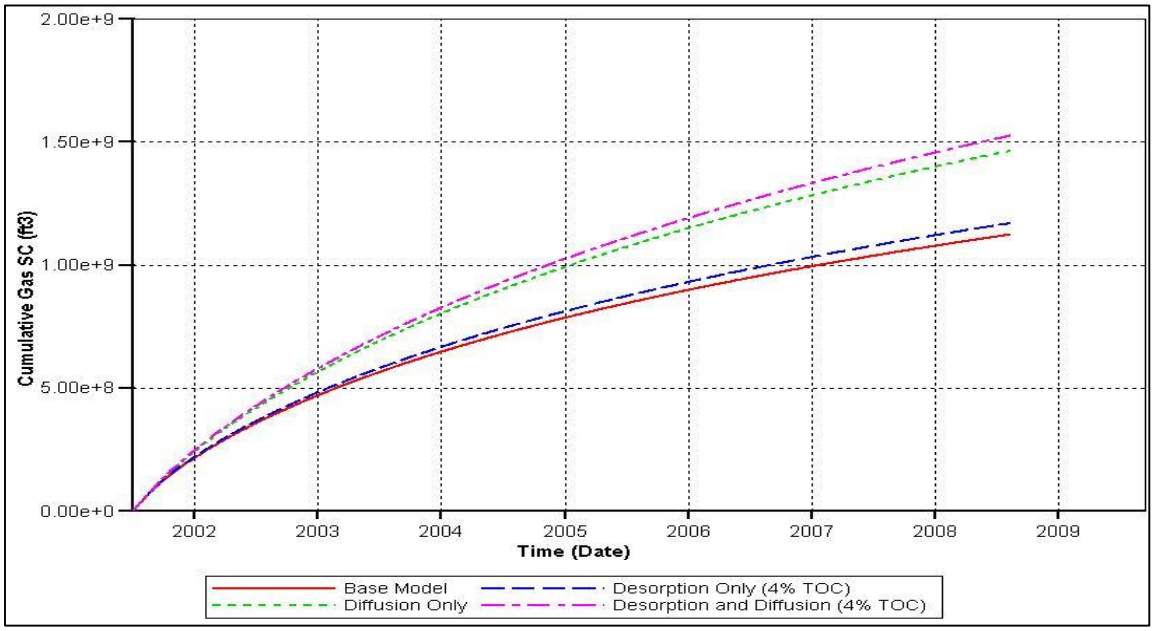


**Figure 26 Cumulative gas production for different cases against the base case.**

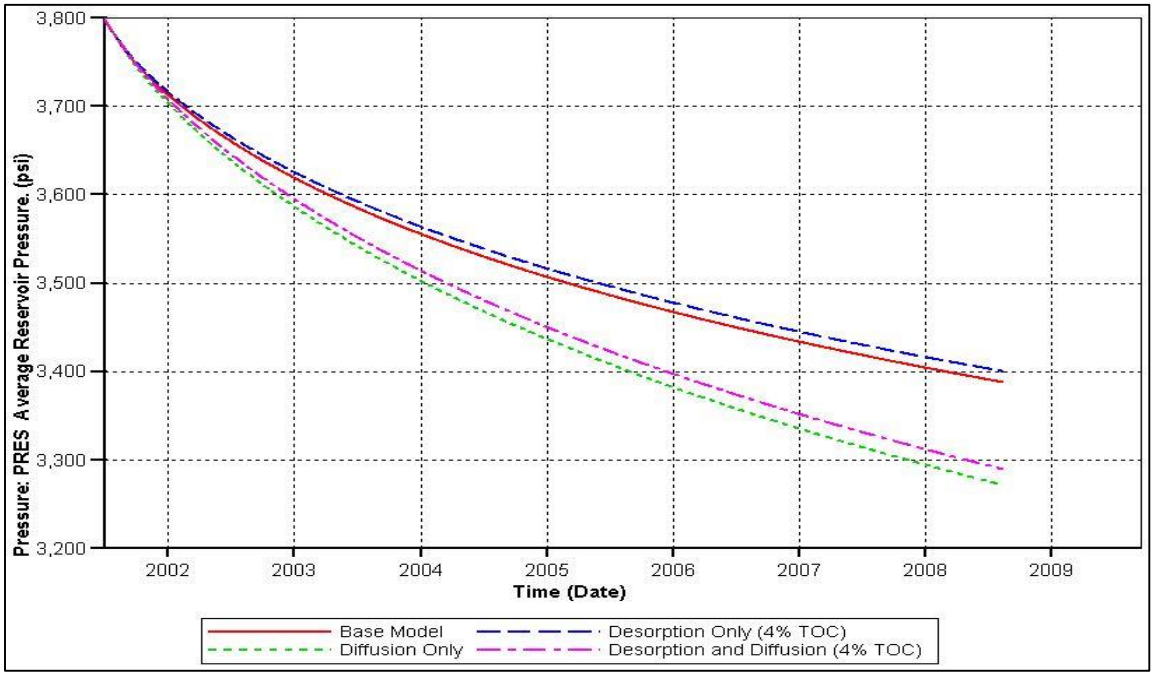


**Figure 27 Average reservoir pressure for different cases.**

Average reservoir pressure for this cases can be seen in Figure 27 as BHP primary constraint. Diffusion causes greater pressure depletion as it helps to produce gas in nano-pores. Desorption helps to maintain pressure but its effect is limited with comparison to diffusion.

Since desorption and diffusion is vital to model shale gas flow, pore size effect and pore volume correction are integrated to the model after desorption and diffusion. These models will be discussed next.

### 4.3. Pore Size Effect

Based on the theoretical background in Chapter III, pore size effect on fluid properties integrated to the simulation model defining another PVT region for the matrix part. Cumulative gas production is expected to decrease as pore width decreases. The reason of this behavior is the decrease of critical temperature and critical pressure of methane depending on pore size.

Cumulative gas production for different cases can be seen in Figure 27. As pore size effects fluid properties, cumulative production decreases as expected. Moreover, decreasing pore size has a great effect on cumulative production as it is seen on the curve for 2.9nm pore width. Deviation begins as the well starts to produce and difference with the cases which are not considering pore size effect is increasing throughout the life of the reservoir. It must be expected that this deviation will be minimized at pressures less than 2000 psi consistently with experimental results.

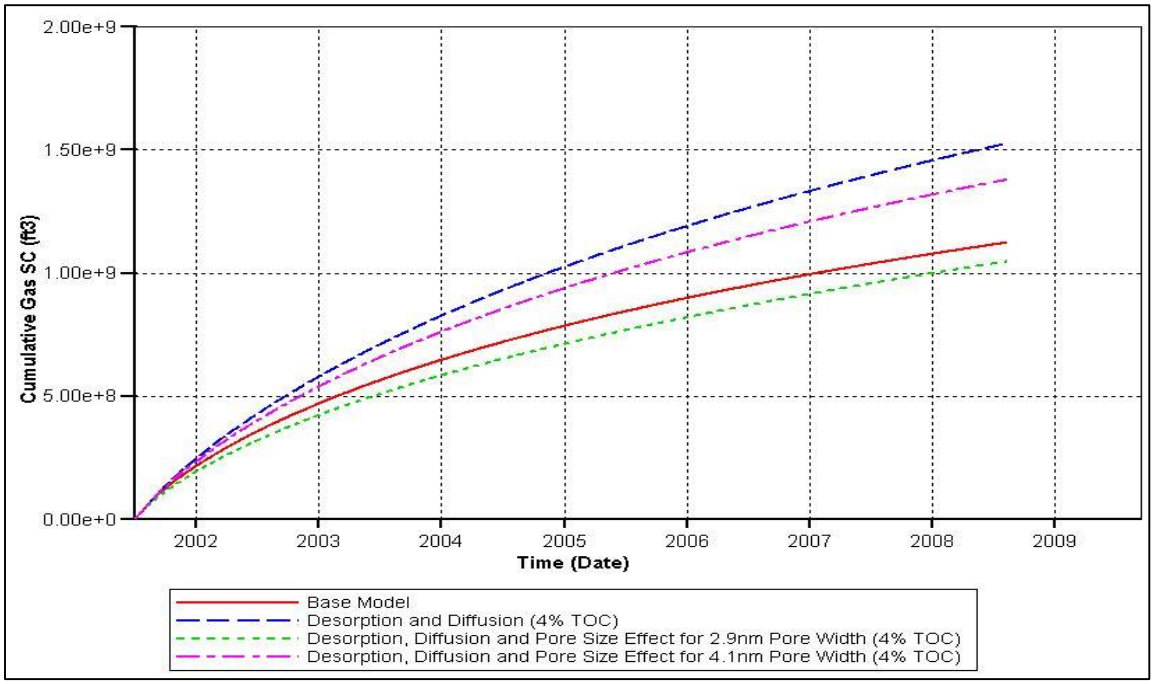


**Figure 28 Cumulative gas production for different cases including pore size effect against the base model.**

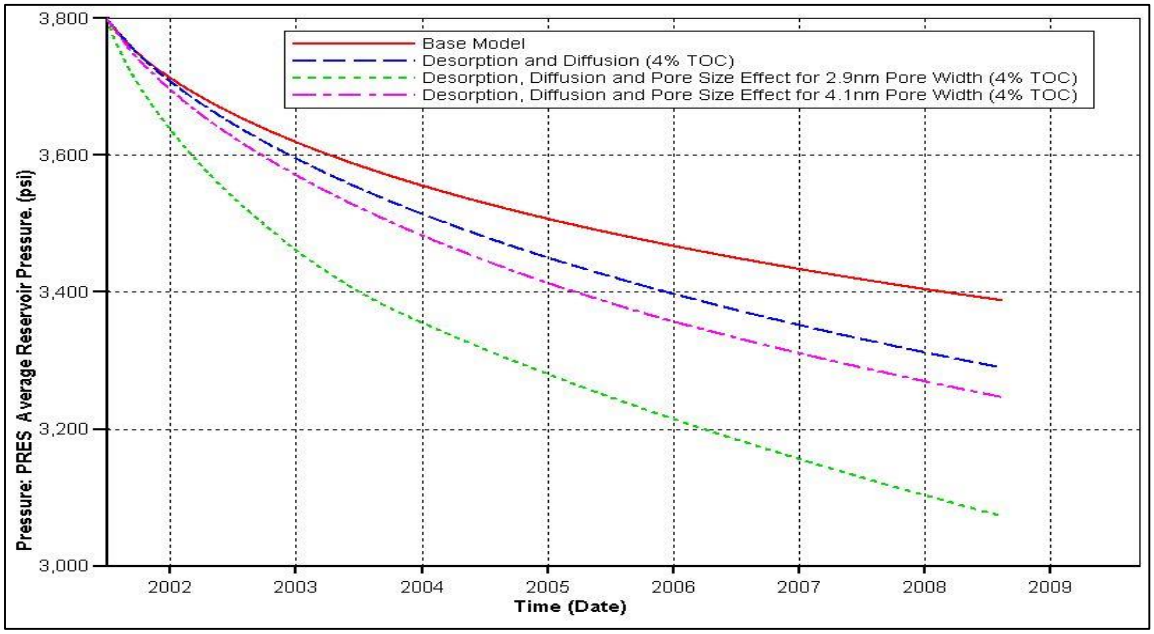


**Figure** 29 **Average reservoir pressure for different cases including pore size effect against the base model.**

Average reservoir pressure for different cases are shown in Figure 28. Base model maintains the highest pressure. It is followed by the case in which desorption and diffusion are integrated to the model. Although desorption is supposed to maintain a high pressure, diffusion causes depletion as it models flow from nano-pores. As pore width decreases, average reservoir pressure decreases as well. It can be concluded that, pore size directly effects the production and reservoir pressure since free gas in place is overestimated without the effect of pore size.

### 4.4. Pore Volume Correction

It is discussed that adsorbed gas occupies considerable part of the pore volume. As pressure decreases, desorbed gas will be produced with free gas, and available pore volume will increase. So it must be modeled depending on pressures as it is discussed in Chapter III.

This phenomenon integrated to the simulation model by modifying Langmuir parameters to mimic the process. Modified Langmuir isotherm captures the pore volume correction. Four different cases are shown in Figure 30. BHP is the primary constraint for all these runs.

Although desorption and diffusion increase the cumulative production, pore size effect causes a considerable decrease. After integrating the pore volume correction, cumulative gas production decreases as expected. Even the effect is limited, it is not negligible. As discussed before, this is because of the occupied pore volume by the adsorbed phase.

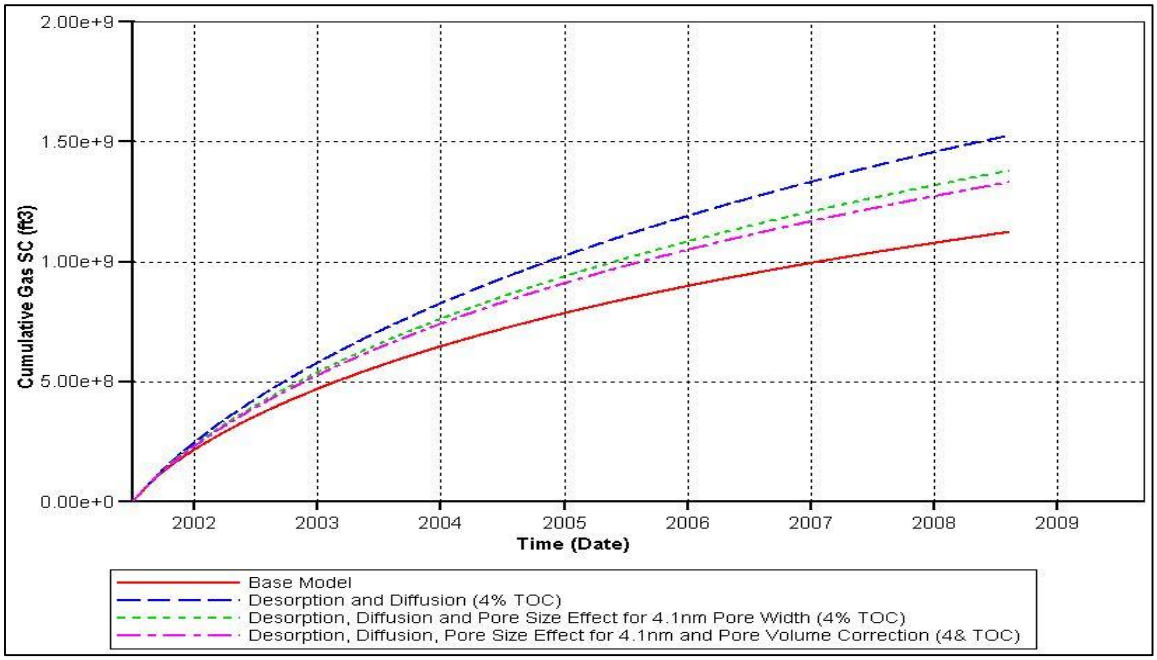


**Figure 30 Cumulative gas production for different cases.**

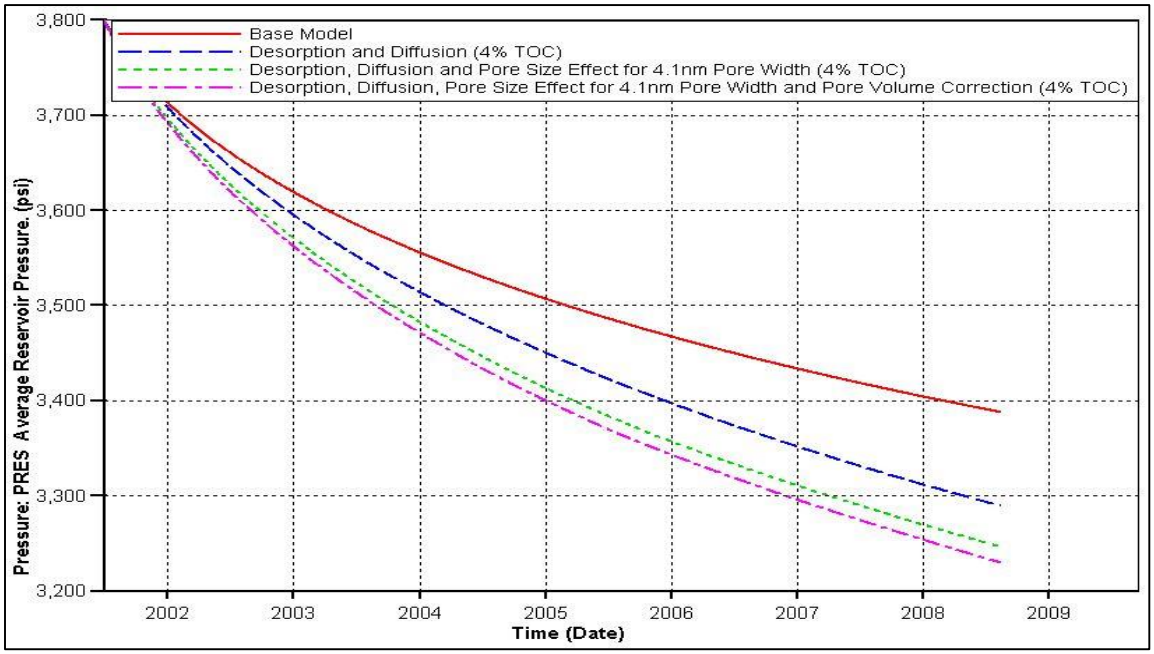


**Figure 31 Average reservoir pressure for different cases.**

In Figure 31, average reservoir pressure profiles of four different cases can be seen. Pore volume correction causes an additional pressure drop since Langmuir parameters are modified to represent the changed Langmuir isotherm. Decline of the adsorbed gas amount causes this drop since there is less gas to maintain pressure.

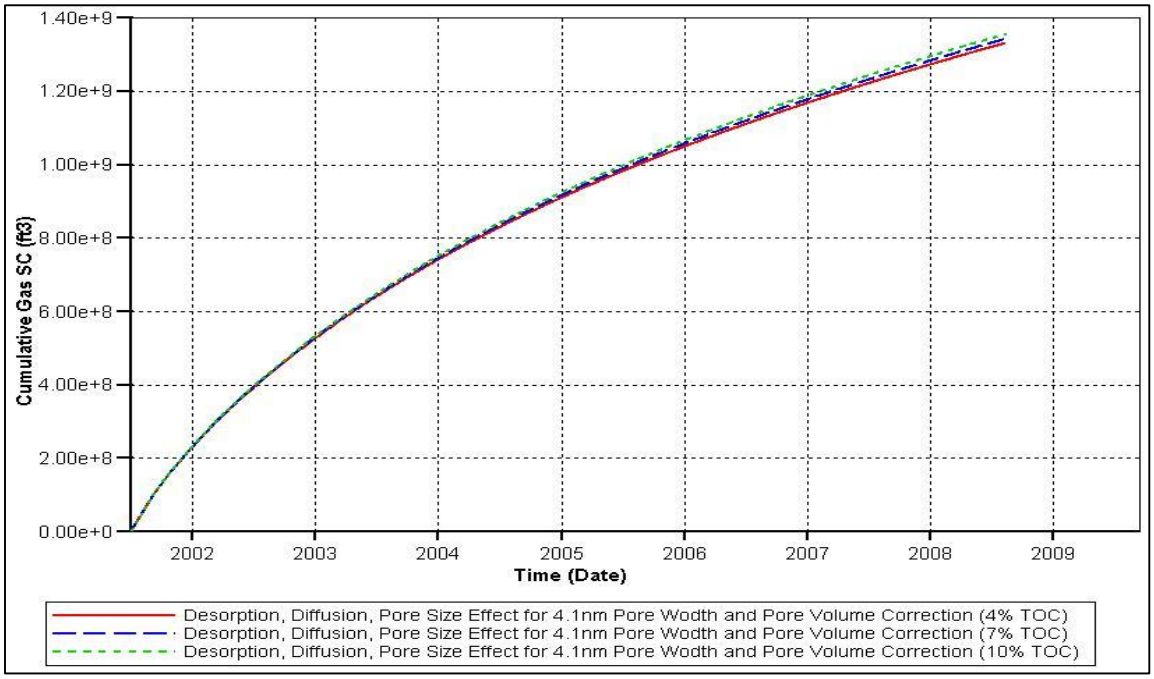


**Figure 32 Cumulative gas production for different TOC.**

Figure 32 shows the difference of the final model for different TOC values. It is interesting to see that the lines are almost overlapped. Separation of these curves is limited with respect to the cases without pore volume correction. Higher TOC means higher adsorbed volume and higher adsorbed volume occupies more pore volume. Thus, higher TOC causes additional decrease on gas in place resulting the convergence of the cumulative gas production. However, higher TOC still gives higher cumulative gas

production as expected. This is because the density of the adsorbed phase is higher than the density of free gas.

Figure 33 shows the average reservoir pressure for different TOC values. The difference between pressure profiles is limited as well. However, higher TOC value still maintains higher average reservoir pressure.

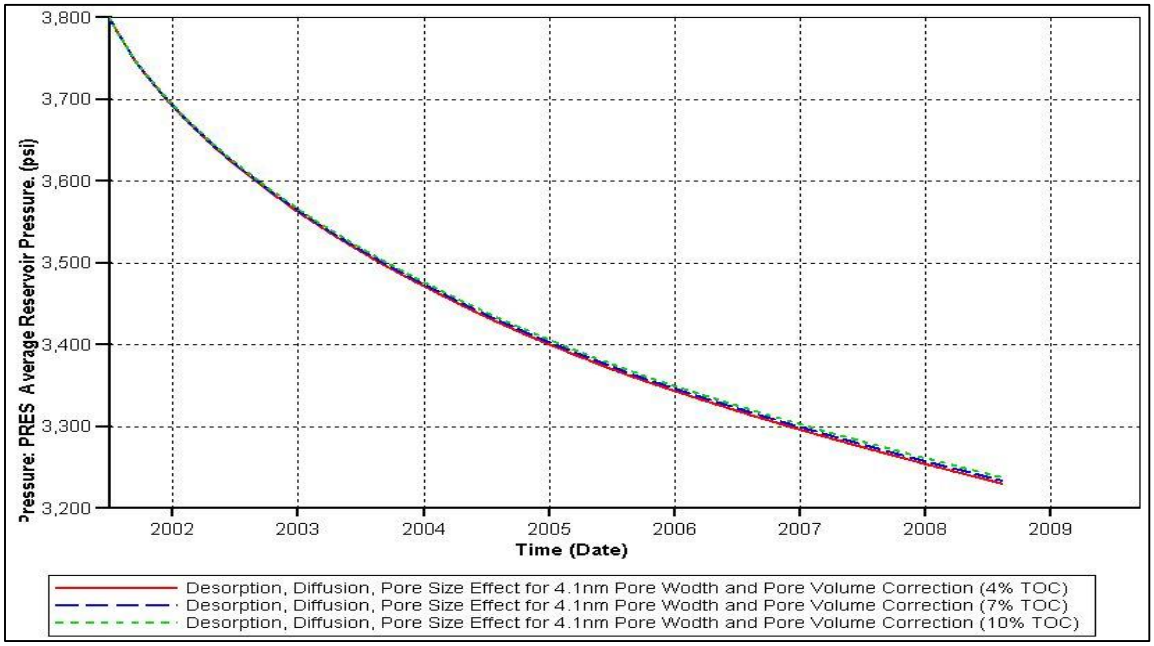


**Figure 33 Average reservoir pressure for different TOC. BHP is primary constraint.**

Pressure profiles of the entire reservoir after 8 years for four different cases can be seen through Figure 34-37. In all cases, pressure drop is mainly between the fracture wings. In Figure 35, it can be seen that the pressure drop in the matrix part between natural fractures is higher than the base model. It is because diffusion helps to drain matrix. Thus, pressure drop reaches that region. Although pressure drop is increased in other cases, pressure profile shows the same characteristics.

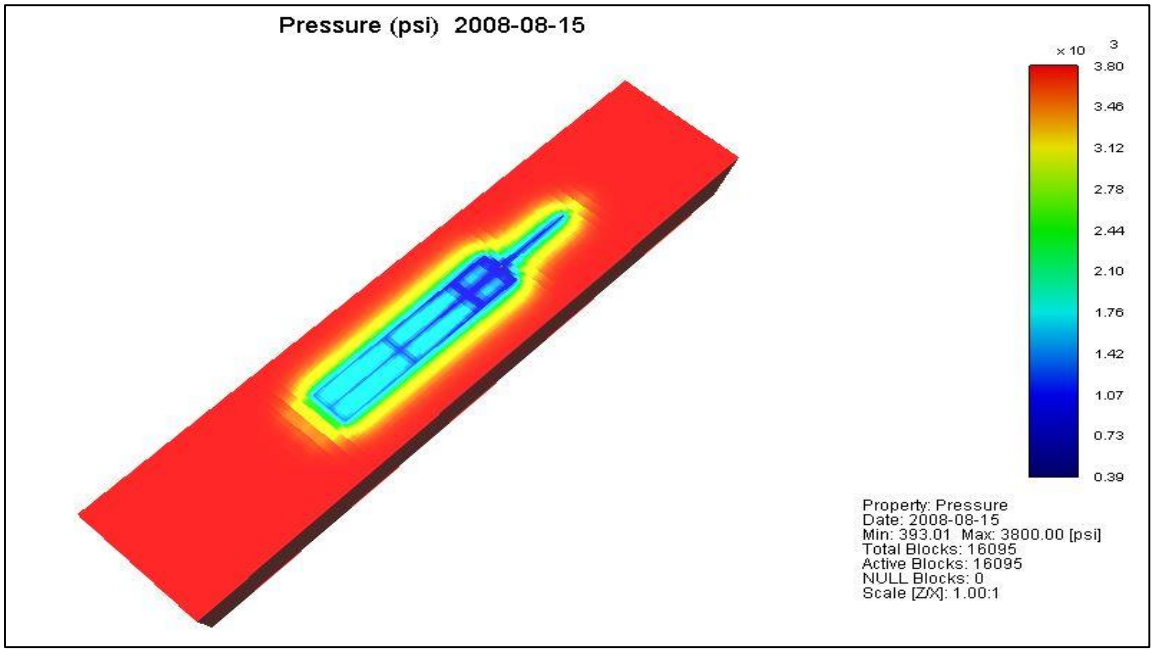


**Figure 34 Reservoir pressure profile of base model after 8 years.**

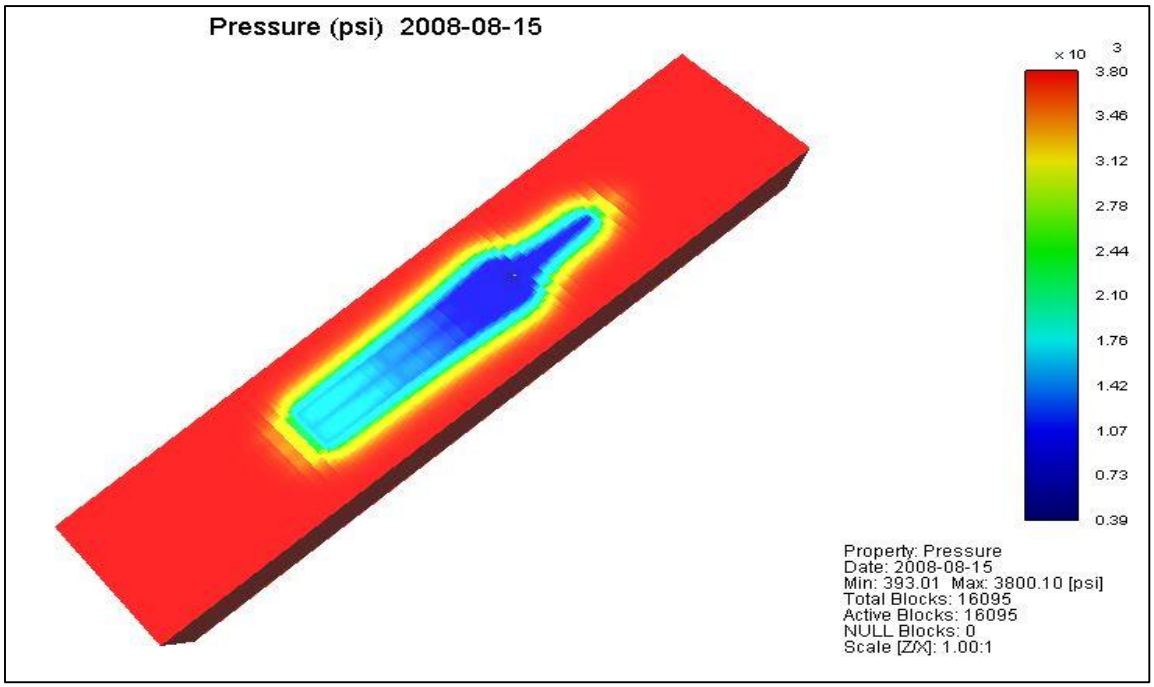


**Figure 35 Reservoir pressure profile of desorption and diffusion integrated model after 8 years.**

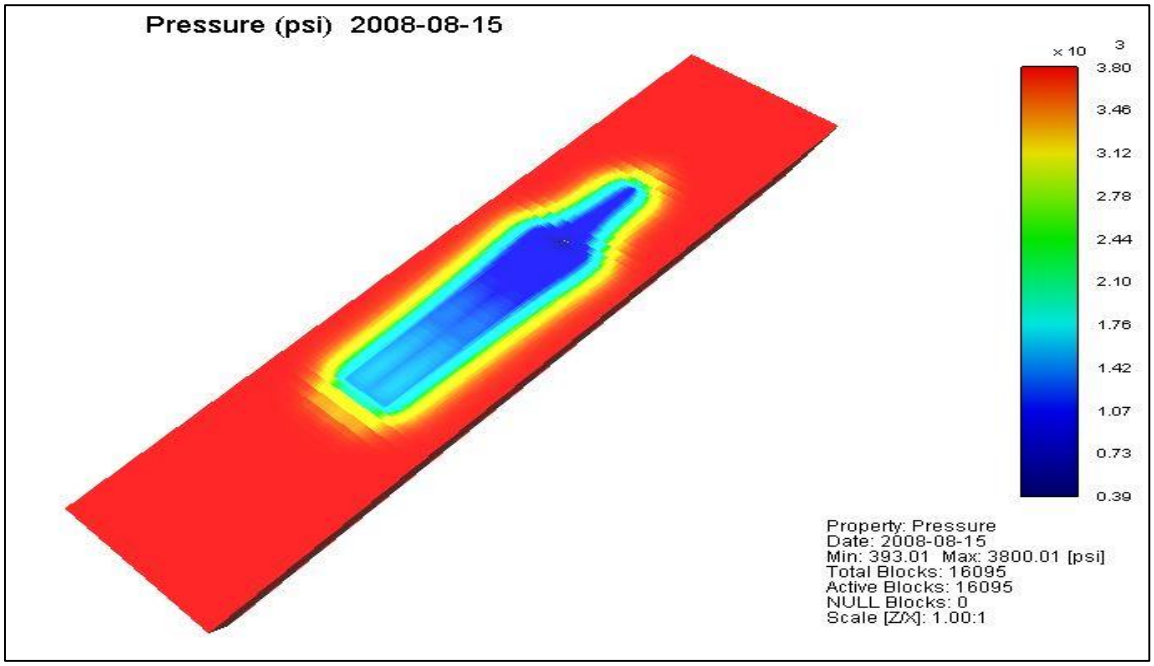


**Figure 36 Reservoir pressure profile of desorption, diffusion and pore size effect integrated model after 8 years.**

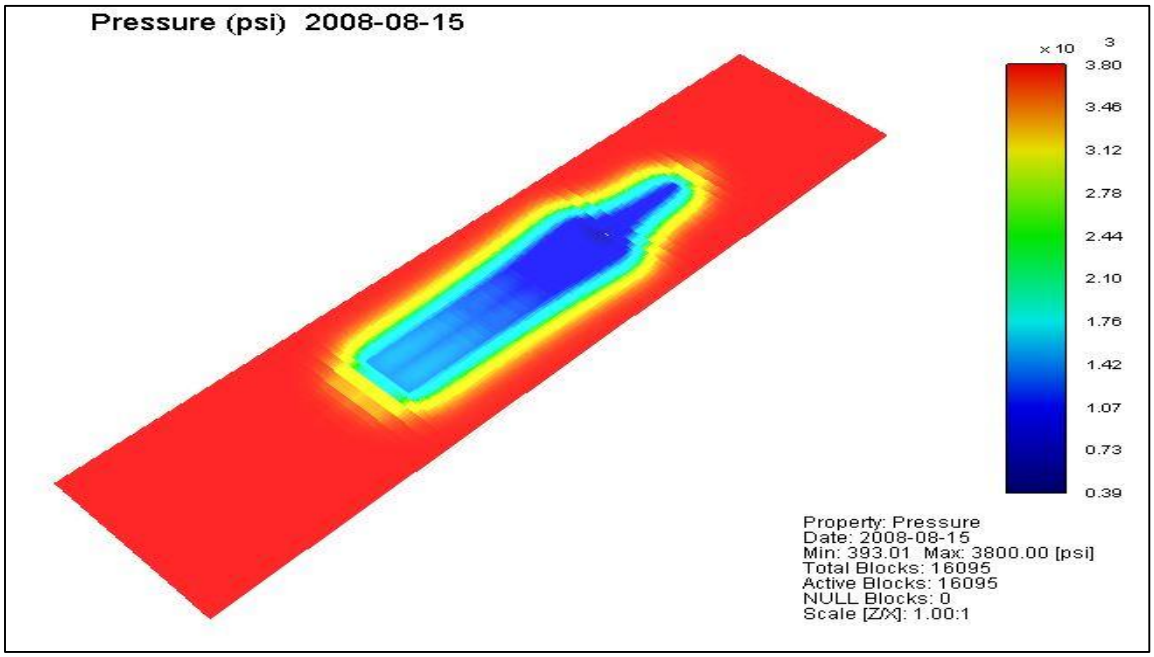


**Figure 37 Reservoir pressure profile of desorption, diffusion, pore size effect and pore volume correction integrated model after 8 years**

## 4.5. Sensitivity Analysis

Final reservoir model includes desorption, diffusion, pore size effect on fluid properties, and pore volume correction for adsorbed phase. This model is used for sensitivity analysis of several parameters which are matrix porosity, natural and hydraulic fracture permeability, minimum bottom hole pressure, Langmuir pressure and Langmuir volume. This study is performed by CMOST module of CMG to determine the effect of parameters on output. This will help to perform history matching study later.

Fracture half length, spacing and extend are not considered as tuning parameters for this run since they are modelled by micro-seismic survey data.

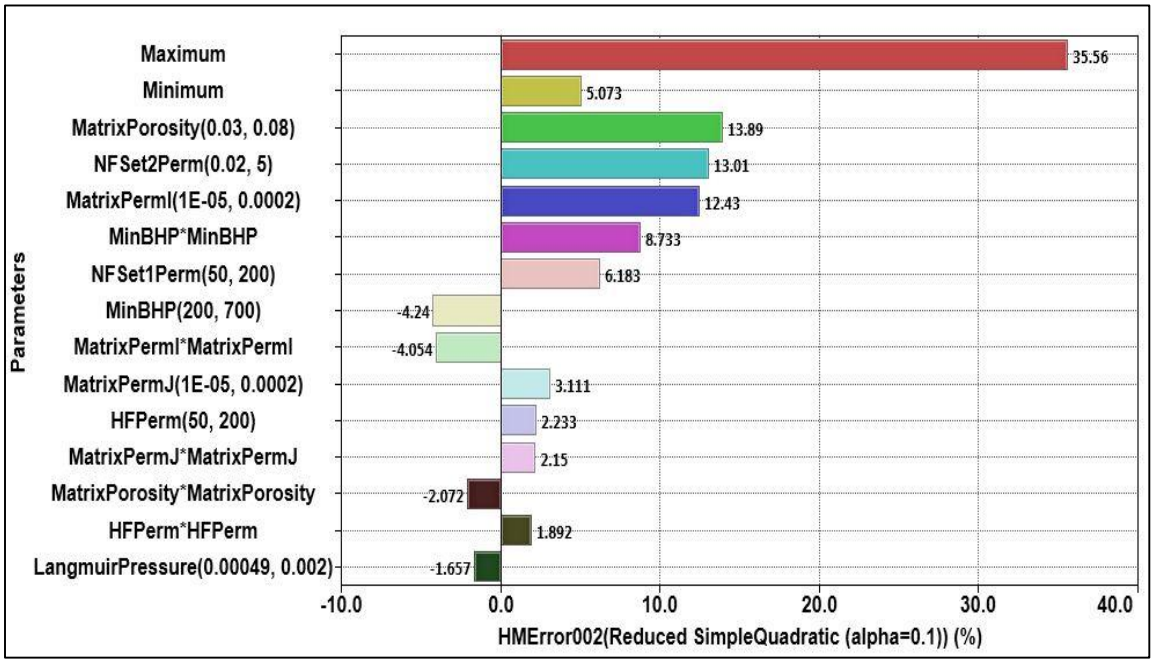


**Figure 38 Tornado plot for well head pressure**

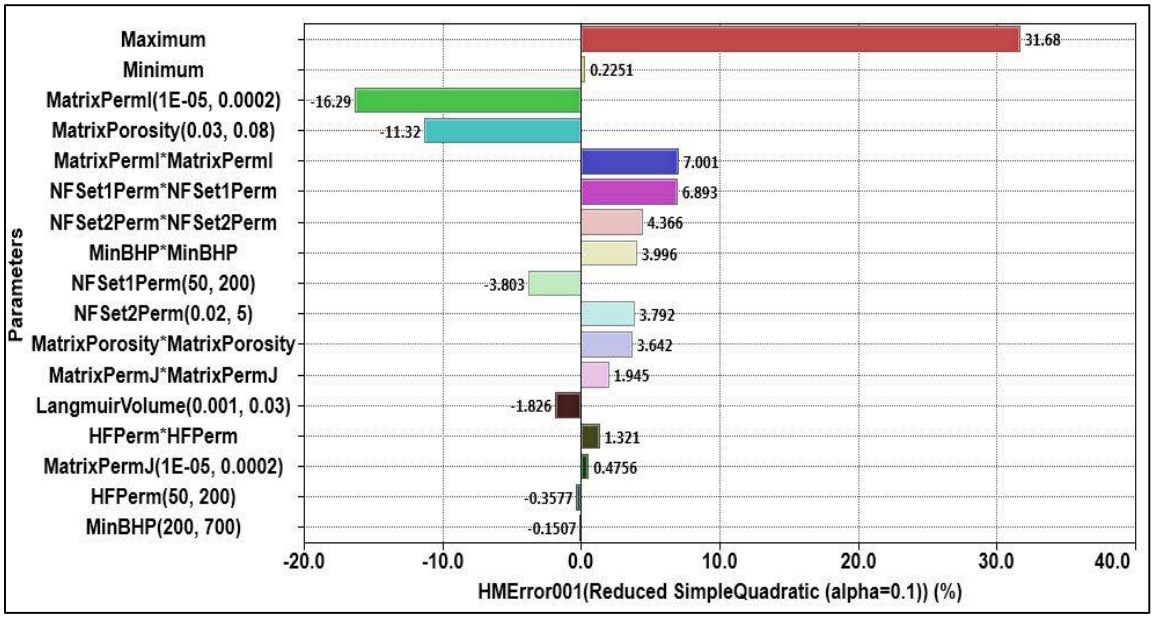


**Figure 39 Tornado plot for cumulative gas production**

Results can be seen in Figure 38 and Figure 39 as tornado plot separately for well head pressure and cumulative gas production respectively. Matrix porosity has the highest impact on well head pressure since it affects original gas in place and cumulative production directly. It is followed by natural fracture and matrix permeability. Cumulative gas production is mainly affected by matrix porosity and permeability. Minimum bottom bole pressure another important parameters for both well head pressure and cumulative gas production.

## 4.6. History Matching

The objective of the history matching in this study is to match well head pressure. Since the model is constrained to gas rate, gas rate would match automatically once the well head pressure is matched.

To be able to perform history match, an objective function which measures the relative difference between field data and simulation results is defined. CMG DECE optimizer is used for this purpose. The process can be described as iterative optimization. The measurement error and weights which are used for objective function can be seen on Table 4. It should be noted that cumulative gas production is used for history matching study instead of gas rate since gas rate is a discontinuous function. Matching the cumulative gas production curve will guarantee the match of gas rate curve.

**Table 4 Error and weight data for history matching objective function.**

| | Absolute Measurement Error | Weight |
|---|---|---|
| Cumulative Gas SC | 0 | 3 |
| Well Head Pressure | 0 | 2 |

Matrix porosity, matrix permeability, natural and hydraulic fracture permeability, minimum bottom hole pressure, Langmuir pressure, and Langmuir volume are set as history matching parameters depending on sensitivity analysis. Upper and lower limit of reservoir properties during history match study can be seen on Table 5.

Results of the history matching study can be seen through Figure 40-42. The improvement on well head pressure match is mostly due to integration of desorption and diffusion. However, pore size effect on fluid properties and pore volume correction for adsorbed phase also helped to get better results.

**Table 5 Upper and lower limits of history matching parameters**

| | Minimum | Default Value | Maximum | Final Value |
|---|---|---|---|---|
| Matrix Porosity | 0.04 | 0.08 | 0.12 | 0.0408 |
| Matrix Permeability | 0.00001 | 0.0001 | 0.001 | 0.0000595 |
| Hydraulic Fracture Permeability (mD) | 50 | 132 | 200 | 123.5 |
| Natural Fracture Permeability, Set1 (mD) | 50 | 81.5 | 200 | 140.75 |
| Natural Fracture Permeability, Set2 (mD) | 0.02 | 0.05 | 5 | 2.6096 |
| Minimum BHP (Psi) | 200 | 393 | 700 | 540 |
| Langmuir pressure (Psi) | 500 | 585 | 2040 | 1262 |
| Langmuir volume (scf/ton) | 2 | 19.74 | 60 | 15.92 |

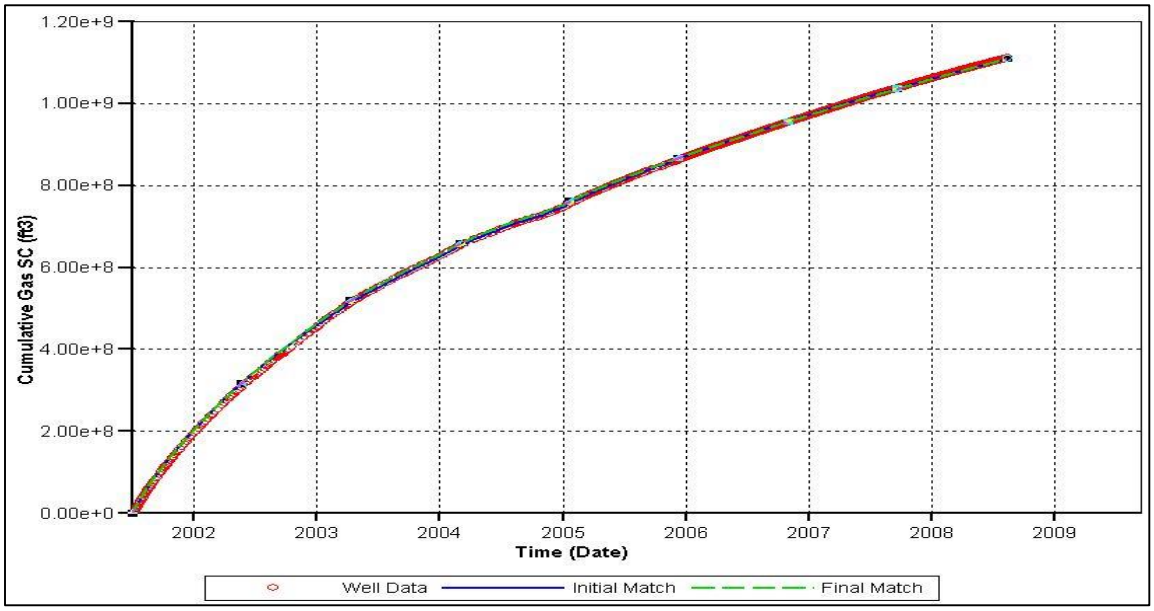


**Figure 40 Cumulative gas production of final model after history match**

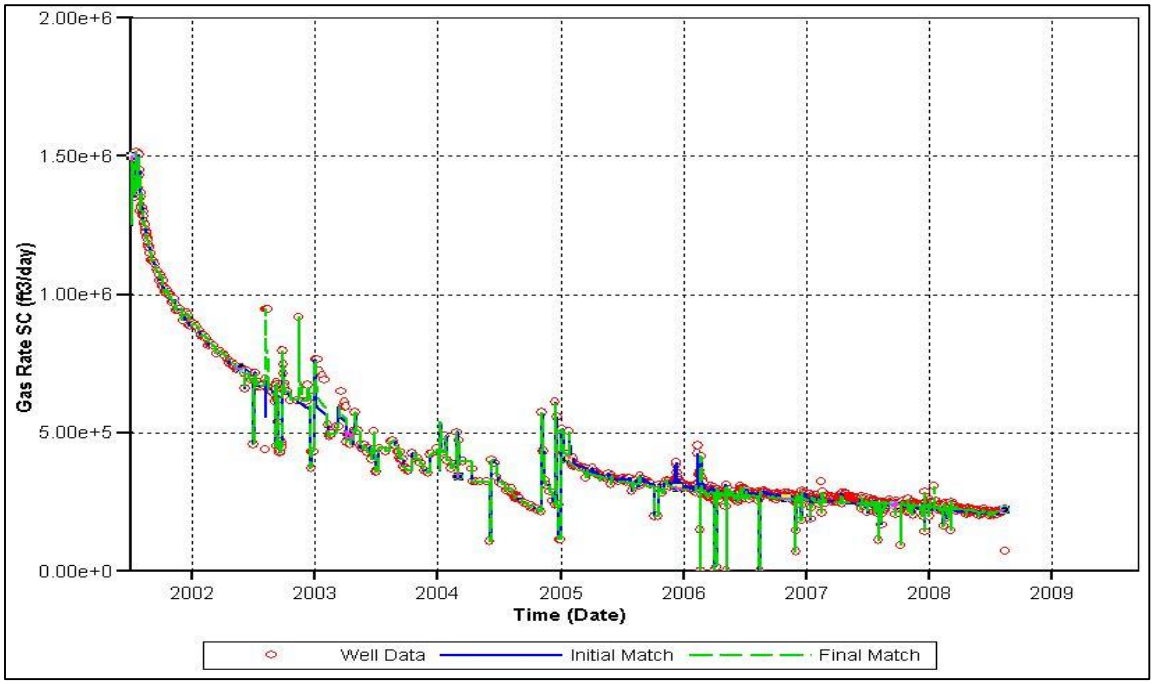


**Figure 41 Gas rate of final model after history match**

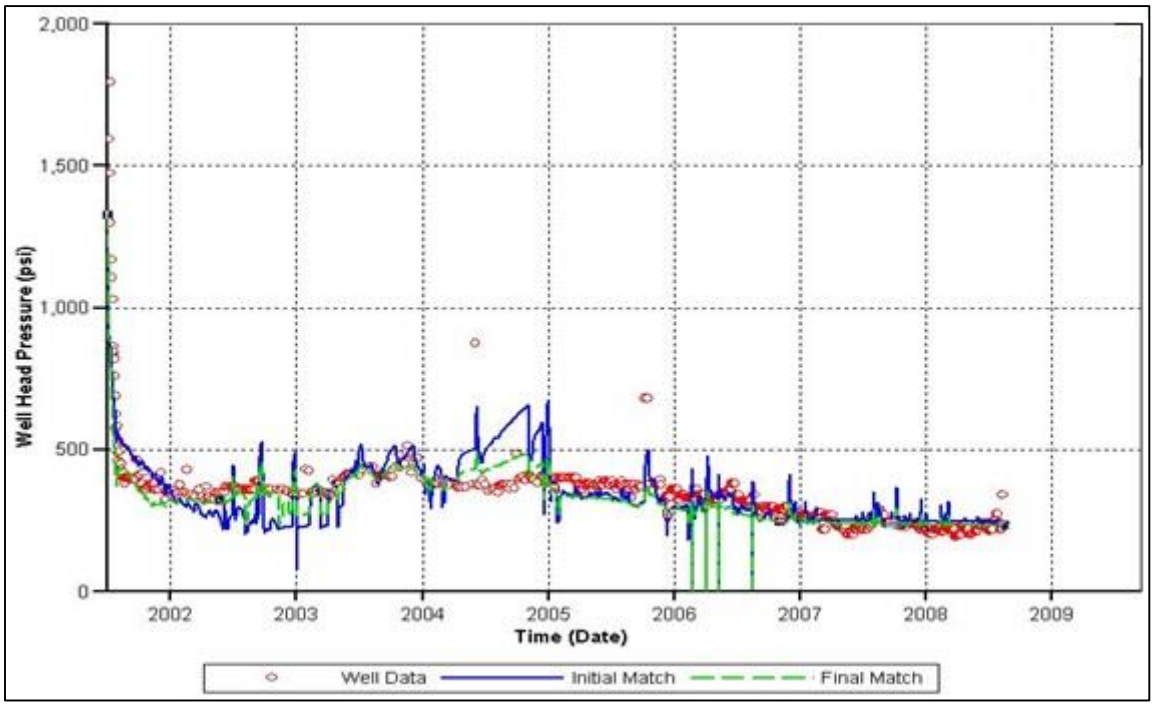


**Figure 42 Well head pressure for final model after history match**

## 4.7. Production Forecast

Cumulative gas production forecast after 30 years can be seen in Figure 43. There is a 30% increase on ultimate recovery at the end of this period. It is important to note that production curves are still not horizontal which represent that the production is still in the economic range. The difference between two models is mainly diffusion. Integrating diffusion into the model provides drainage from nano-pores and increases the ultimate recovery. Because of very low permeability, pressure decrease does still not reach to the boundaries of the reservoir volume. Desorption also helps to increase the recovery.

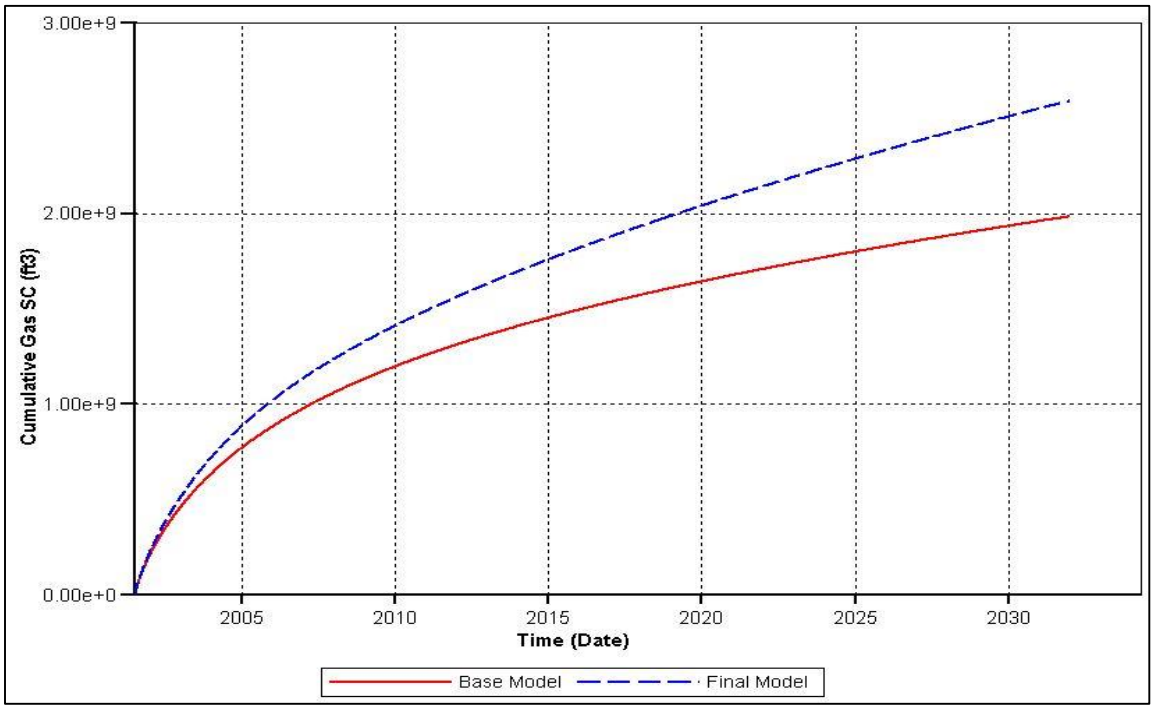


**Figure 43 Cumulative gas production after 30 years of production with constant BHP**

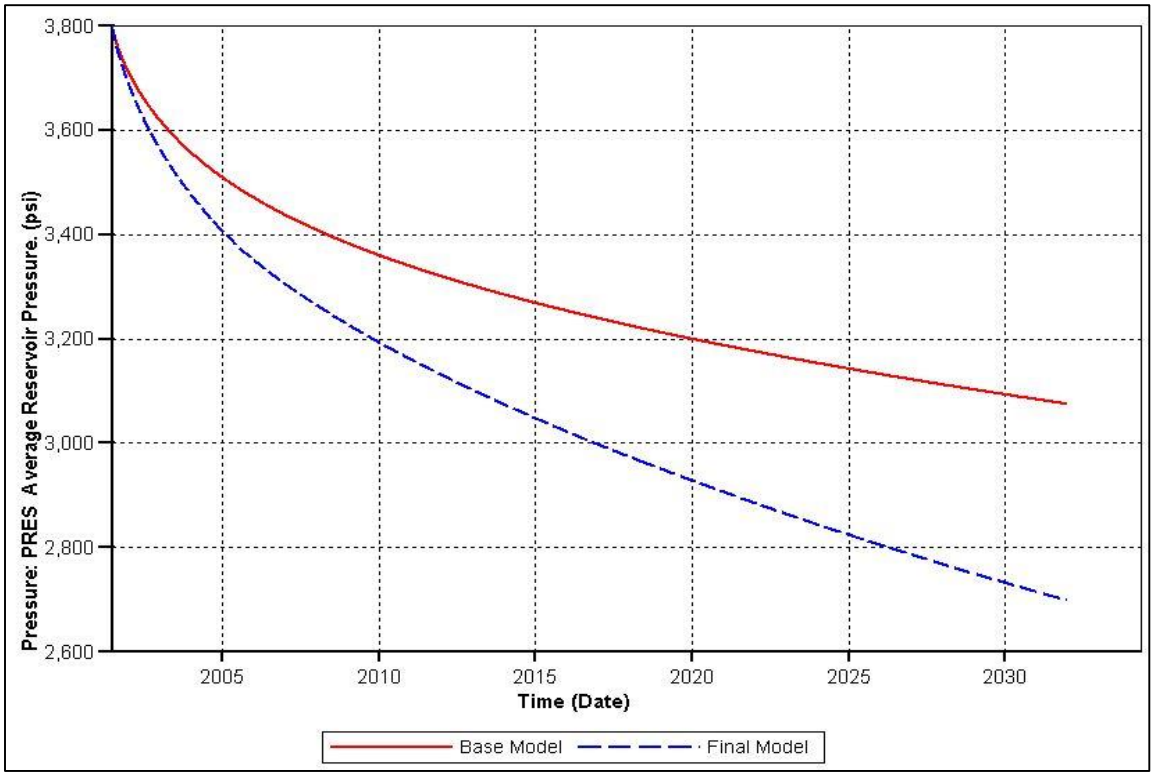


**Figure 44 Average reservoir pressure after 30 years of production with constant BHP**

Average reservoir pressure after 30 years can be seen in Figure 44. Final model shows an important decrease on average reservoir pressure with the same reason as discussed above. Figure 45 and 46 show the reservoir pressure profile after 30 years of production with constant BHP for base model and final model respectively. As it is seen, pressure decrease of base model is limited with the volume between natural fracture wings. On the other hand, final model shows more pressure decrease beyond fracture wings due to modeling gas drainage from nano-pores with diffusion. Although its effect is limited, pore size effect and pore volume correction are also important to accurately model the process.

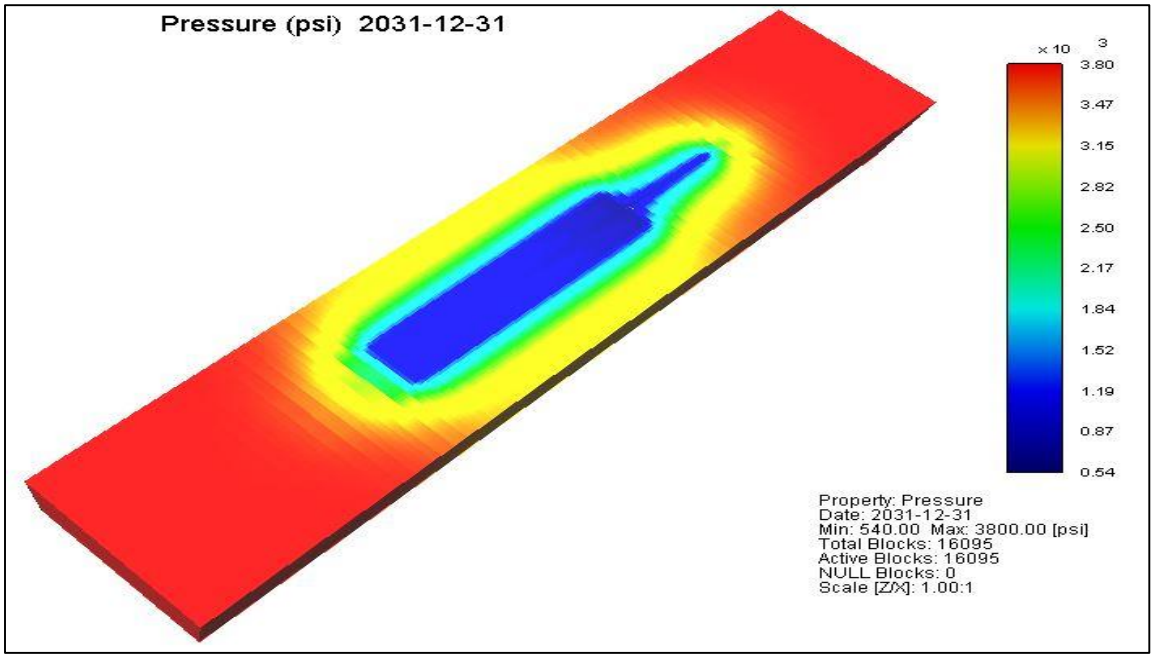


**Figure 45 Reservoir pressure profile after 30 years of production with constant BHP**

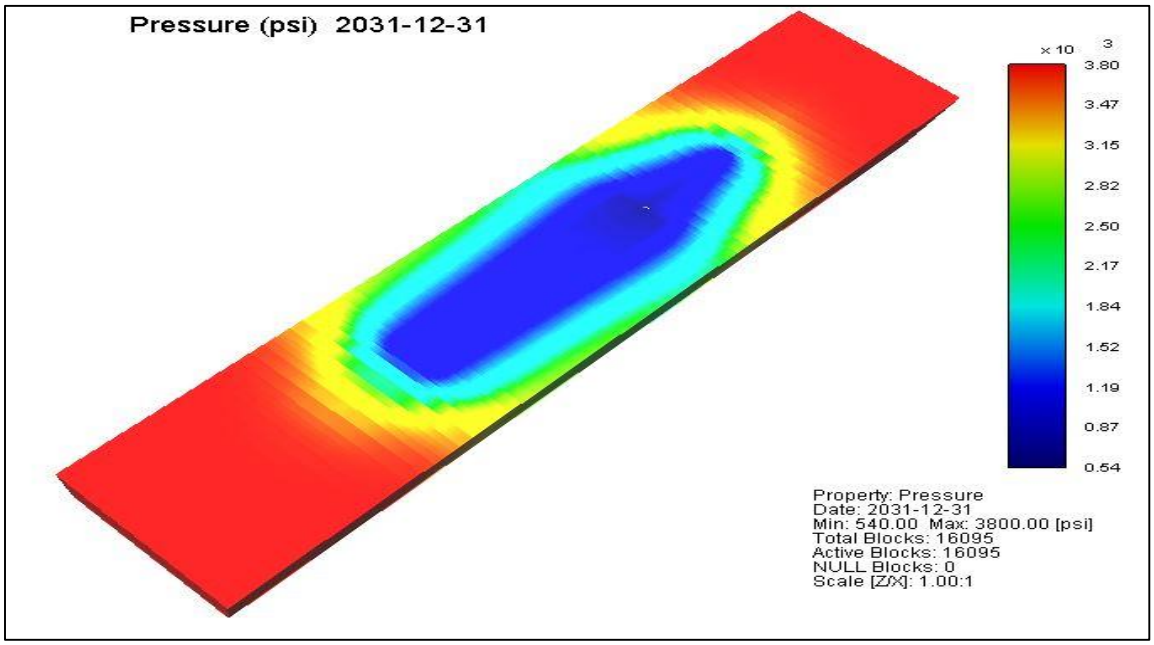


**Figure 46 Reservoir pressure profile after 30 years of production with constant BHP**

# CHAPTER V

# CONCLUSIONS

This study focuses on the reservoir simulation of shale gas flow. Different flow and storage mechanisms are integrated to the reservoir model. After integrating desorption and diffusion, pore size effect on fluid properties and pore volume correction for adsorbed phase are considered to improve the model.

It is observed that adsorption is an important storage mechanism which increases gas in place reserves estimation. Even though it has a limited effect on gas production because of low matrix permeability, it must still be taken into consideration. However, integrating desorption into the simulation model requires a special attention since adsorbed gas occupies some of the pore volume.

Diffusion integrated to the simulation model by using the idea of apparent dynamic permeability. It is shown that diffusion helps to increase drainage from extensive nano and micro pores. Without considering diffusion, simulation model is not able to drain low permeability matrix.

Another consideration is pore size effect on gas properties. Decreasing pore size has a strong effect on gas formation volume factor and viscosity. It causes a decrease on cumulative gas production and average reservoir pressure.

Nano-scale effects have a huge impact on both cumulative gas production and reservoir pressure. As a result, accurate modeling and reducing uncertainity require special attention on desorption, diffusion, pore size effect, and pore volume correction.

# REFERENCES


Adesida, A. G., Akkutlu, I. Y., Resasco, D. E. et al. 2011. Characterization of Barnett Shale Kerogen Pore Size Distribution using DFT Analysis and Grand Canonical Monte Carlo Simulations. Presented at SPE Annual Technical Conference and Exhibition, Denver, Colorado, USA, 30 October - 2 November. SPE-147397-MS. http://dx.doi.org/10.2118/147397-MS.

Ambrose, R. J., Hartman, R. C., Diaz-Campos, M. et al. 2012. Shale Gas-in-Place Calculations Part I: New Pore-Scale Considerations. *SPE Journal* **17** (01): 219-229. SPE-131772-PA. http://dx.doi.org/10.2118/131772-PA.

Boyer, C., Kieschnick, J., Rivera, R. S. et al. 2006. Producing Gas from Its Source. *Oilfield Review* **18** (3).

Carlson, E. S. and Mercer, J. C. 1991. Devonian Shale Gas Production: Mechanisms and Simple Models. *Journal of Petroleum Technology* **43** (04). SPE-19311-PA. http://dx.doi.org/10.2118/19311-PA.

Curtis, M. E., Ambrose, R. J., and Sondergeld, C. H. 2010. Structural Characterization of Gas Shales on the Micro- and Nano-Scales. Presented at Canadian Unconventional Resources and International Petroleum Conference, Calgary, Alberta, Canada, 19-21 October. SPE-137693-MS. http://dx.doi.org/10.2118/137693-MS.

Didar, B. R. and Akkutlu, I. Y. 2013. Pore-Size Dependence of Fluid Phase Behavior and the Impact on Shale Gas Reserves. Presented at Unconventional Resources

Technology Conference, Denver, Colorado, USA, 12-14 August. SPE-168939-MS. http://dx.doi.org/10.1190/URTEC2013-183.

Ertekin, T., King, G. A., and Schwerer, F. C. 1986. Dynamic Gas Slippage: A Unique Dual-Mechanism Approach to the Flow of Gas in Tight Formations. *SPE Formation Evaluation* **1** (01). SPE-12045-PA. http://dx.doi.org/10.2118/12045-PA.

Farid, S. M. U. 2015. *Modelling Shale Gas Flow Using The Idea of Dynamic Apparent Permeability*. MS Thesis, Texas A&M University, College Station, Texas, USA (June 2015).

Hill, D. G. and Nelson, C. R. 2000. Gas Productive Fractures Shales - and Overview and Update *Gas TIPS* **6** (2): 4-13.

Jarvie, D. M., Hill, R. J., Pollastro, R. M. et al. Evaluation of hydrocarbon generation and storage in Barnett Shale, Fort Worth basin. *Brookhaven College, TX, USA*, 2-5.

Jarvie, D. M., Hill, R. J., Ruble, T. E. et al. 2007. Unconventional shale-gas systems: the Missipian Barnett Shale of north-central Texas as one model for thermogenic shale-gas assessment. *American Association Petroleum Geologists Bulletin* **91**: 475-499.

Javadpour, F. 2009. Nanopores and Apparent Permeability of Gas Flow in Mudrocks (Shales and Siltstone). *Journal of Canadian Petroleum Technology* **48** (08). PETSOC-09-08-16-DA. http://dx.doi.org/10.2118/09-08-16-DA.

Javadpour, F., Fisher, D., and Unsworth, M. 2007. Nanoscale Gas Flow in Shale Gas Sediments. *Journal of Canadian Petroleum Technology* **46** (10): 55-61. PETSOC-07-10-06. http://dx.doi.org/10.2118/07-10-06.

Mayerhofer, M. J., Lolon, E. P., Youngblood, J. E. et al. 2006. Integration of Microseismic-Fracture-Mapping Results With Numerical Fracture Network Production Modeling in the Barnett Shale. Presented at SPE Annual Technical Conference and Exhibition San Antonio, Texas, USA, 24-27 September. SPE-102103-MS. http://dx.doi.org/10.2118/102103-MS.

Montgomery, S. L., Jarvie, D. M., Bowker, K. A. et al. 2005. Mississippian Barnett Shale, Fort Worth Basin, North-Central Texas: Gas-Shale Play with Multi-Trillion Cubic Feet Potential. *AAPG Bulletin* **89** (02): 155-175. 10.1306/09170404042.

Passey, Q. R., Moretti, F. J., Kulla, J. B. et al. 1990. A practical model for organic richness from porosity and resistivity logs. *AAPG Bulletin* **74** (12): 1777-1794. 5682561.

Santos, J. M. and Akkutlu, I. Y. 2013. Laboratory Measurement of Sorption Isotherm under Confining Stress with Pore-Volume Effects. *SPE Journal* **18** (05): 924-931. SPE-162595-PA. http://dx.doi.org/10.2118/162595-PA.

Shabro, V., Torres-Verdin, C., and Sepehrnoori, K. 2012. Forecasting Gas Production in Organic Shale with the Combined Numerical Simulation of Gas Diffusion in Kerogen, Langmuir Desorption from Kerogen Surfaces, and Advection in Nanopores. Presented at SPE Annual Technical Conference and Exhibition, San

Antonio, Texas, USA, 8-10 October. SPE-159250-MS. http://dx.doi.org/10.2118/159250-MS.

Sing, K. S. W., Everett, D. H., Haul, R. A. W. et al. 1985. Reporting Physisorption Data for Gas/Solid Systems with Special Reference to the Determination of Surface Area and Porosity *Pure Appl. Chem.* **57** (4): 603-619.

Williams, J. L. 2015. US Rotary Rig Count, http://www.wtrg.com/rotaryrigs.html.

Yan, B., Killough, J. E., Wang, Y. et al. 2013a. Novel Approaches for the Simulation of Unconventional Reservoirs. Presented at Unconventional Resources Technology Conference, Denver, Colorado, USA, 12-14 August. SPE-168786-MS. http://dx.doi.org/10.1190/URTEC2013-131.

Yan, B., Wang, Y., and Killough, J. E. 2013b. Beyond Dual-Porosity Modeling for the Simulation of Complex Flow Mechanisms in Shale Reservoirs. Presented at SPE Reservoir Simulation Symposium, The Woodlands, Texas, USA, 18-20 February. SPE-163651-MS. http://dx.doi.org/10.2118/163651-MS.

Zhang, T., Ellis, G. S., C., R. S. et al. 2012. Effect of Organic Matter Type and Thermal Maturity on Methane Adsorption in Shale Gas Systems. *Organic Geochemistry* **47**: 120-131.